Measuring Marine Currents Using Underwater Acoustics

by

© **Tim A. Smith**

A thesis submitted to the School of Graduate Studies in partial fulfillment of the requirements for the degree of Master of Engineering.

Faculty of Engineering and Applied Science

Memorial University

May 2020

St. John's, Newfoundland and Labrador, Canada

Abstract

The speed of sound in water rises and falls with temperature, current speed, salinity, and pressure. Precisely measured underwater acoustic travel times can be used to calculate these parameters for a body of water. If the salinity and pressure along the acoustic path is known, a system of two underwater hydrophones transmitting bi-directionally can indirectly measure both temperature and water velocity. Summing the bi-directional travel times isolates the temperature component, while subtracting the travel times isolates the component of current speed.

There has been much work in using this method for current point detectors as well as networks covering very large distances (> 100km). The feasibility of using acoustic travel times for measurements in the 100m - 3km range has been less explored. Accurate measurements at this range may be valuable in iceberg tracking for the offshore oil and gas industry, as well as in building high resolution maps for environmental studies. This range presents some new challenges, as a distributed network must remain highly synchronized to obtain sufficiently accurate travel times. Multipath travel is also highly problematic in this range.

A system has been developed and used to measure tidal currents in the North Atlantic Ocean. The design was built from the ground up. The hardware, software, and data processing are built to work with non-specialized low-cost equipment in a variety of harsh marine deployment conditions. Field testing showed that the system was capable of measuring currents to within $\pm 4 cm/s$ across a 130m range. Quantitative error analysis is included which shows that much higher accuracies could be achieved at the 1km range.

Acknowledgements

A project of this magnitude requires the support of many people to accomplish. I'd like to take advantage of this space to acknowledge some of those who helped along the way. This list is nowhere near exhaustive but includes a few people who generously gave their time, equipment, knowledge, and labour.

- Dr. Vlastimil Masek and his family
- My wife, Renee
- Mom and Dad
- Paula and the Turners
- Steve and the Smiths
- The team at Setpoint AE
- Ren Hodder and Perry Rees
- The Memorial University Technical Services team

Big thanks to this group and to everyone else who contributed to this work!

Table of contents

Title page i

Abstract ii

Acknowledgements iii

Table of contents iv

List of figures vi

List of symbols viii

List of abbreviations ix

1 Introduction 1

1.1 Problem Statement 2

1.2 Contributions 4

1.3 Organization 5

2 Background 6

2.1 Acoustic Wave Propagation in Water 7

2.2 History of Acoustic Travel Time Current Sensing 12

2.3 Other Current Sensing Methods 14

2.4 Commercially Available Acoustic Travel Time Devices 16

3 Hardware **17**

3.1 Topology 18

3.2 Power 21

3.3 Microcontrollers 22

3.4 Communications 23

3.5 Hydrophone Interfaces 25

4 Software **31**

4.1 Measurement Sequence 33

4.2 Time Synchronization 36

4.3 Travel Time Calculation 42

4.4 Current and Temperature Measurement 47

4.5 Error Analysis 50

4.6 User Interface 54

5 System Testing **58**

5.1 Lab Verification of Travel Time Accuracy 59

5.2 Long Pond Winter 2019: Measurements Under Ice 63

5.3 Bellevue Summer 2019: Tidal Current Measurement 67

6 Conclusions **73**

6.1 Lessons Learned 74

6.2 Future Work 76

Bibliography **77**

List of figures

2.1 Visual Representation of the Multipath Effect 9

3.1 System Topology 19

3.2 Inter-node Power/Data Bus from Master's Point-of-View 20

3.3 Waveform Capture of the Power/Data Bus (Fig. 3.2 Ch.1: BUS) 20

3.4 Power Conditioning Circuit 21

3.5 Power Supply After Filtering (Fig. 3.4 Ch.1: $V+$) 22

3.6 Data Transmitting and Receiving Circuit 23

3.7 Modulating Outgoing Modbus Transmissions (Fig. 3.6 Ch.1: PT, Ch.2: Tx, Ch.4: B) 24

3.8 Buffering Received RS485 Data (Fig. 3.6 Ch.1: A, Ch.2: B, Ch.4: RO) 25

3.9 Timing Recovery of RS485 Data (Fig. 3.6 Ch.1: $PD+$, Ch.2: $PD-$, Ch.4: Rx) . 25

3.10 Hydrophone Transmitting Circuit 26

3.11 PWM Signal from Microcontroller (Fig. 3.10 Ch.1: PWM) 27

3.12 High Voltage Signal to Hydrophone (Fig. 3.10 Ch.1: $HYDRO$, R1 De-energized) 27

3.13 Attenuated Read-back Signal (Fig. 3.10 Ch.1: $DATA$, R1 De-energized) 28

3.14 Hydrophone Receiving Circuit 29

3.15 Signal Received from Hydrophone (Fig. 3.14 Ch.1: $HYDRO$, R1 Energized) . 29

3.16 Amplified Signal from Hydrophone (Fig. 3.14 Ch.1: $DATA$, R1 Energized) . . 30

4.1 Onshore Master State Transition Diagram 34
4.2 Subsea Node State Transition Diagram 35
4.3 Clock Drift Over a 600ms Time-span 38
4.4 Time Shift and Scaling of a Received Signal 42
4.5 Autocorrelation with Multipath Error 44
4.6 BPSK Sequence Autocorrelation 46

5.1 Travel Time Testing in Lab 60
5.2 Lab Testing of Distance Sensitivity 61
5.3 Distance Based Sensitivity Testing in Lab 62
5.4 Long Pond Testing February 2019 Top-Down View 63
5.5 Long Pond Testing February 2019 Ground Level View 64
5.6 ADCP and Travel Time Based Data Comparison 65
5.7 Long Pond Depth Comparison 66
5.8 Bellevue Testing August 2019 Top-Down View 67
5.9 Bellevue Testing August 2019 Ground Level View 68
5.10 Current and Temperature from Bellevue Testing August 2019 69
5.11 Propeller Strike Effect on Data Quality 71

List of symbols

t_1	Acoustic travel time from node 1 to node 2
t_2	Acoustic travel time from node 2 to node 1
e_t	Error in acoustic travel time measurement
Δt	$t_2 - t_1$
$e_{\Delta t}$	Error in Δt measurement
Σt	$t_1 + t_2$
d	Distance
e_d	Error in distance measurement
c	Sound speed
e_c	Error in sound speed measurement
v	Water velocity (current speed)
e_v	Error in velocity measurement
T	Water temperature
e_T	Error in temperature measurement
S	Salinity
Z	Depth
Φ	Latitude

List of abbreviations

ADC	Analog to Digital Converter
ADCP	Acoustic Doppler Current Profiler
BPSK	Binary Phase Shift Keying
CTD	Conductivity, Temperature, Depth sensor
SPDT	Single Pole Double Throw
GPS	Global Positioning System
OOK	On Off Keying
PWM	Pulse Width Modulation
SNR	Signal to Noise Ratio
USB	Universal Serial Bus

Chapter 1

Introduction

Measurement of physical ocean properties has become a subject of significant research focus over the past century. Quantifying climate change, offshore oil development, and studies of marine wildlife are examples of subject areas which benefit from reliable data on ocean currents and temperatures. It is no surprise then, that there are a wide variety of sensor technologies available to measure these parameters. While improvements in these technologies in recent years have led to a greater understanding of the world's oceans, there is a still a need from the scientific and industrial communities for improvements in instrumentation reliability, accuracy, and cost-effectiveness.

The four characteristic properties which define an area of the ocean are temperature, current velocity, pressure, and salinity. The definition of the range of an area of ocean varies greatly depending on the application. Oceanographers investigating global ocean trends are interested in the mesoscale (100km), the sub-basin scale (>1Mm), and the antipodal scale (>20Mm). An offshore oil platform may be interested in knowing the current speeds within the immediate 3km radius to the assess the risk of collision with an iceberg or alongside

vessel. Utilities, such as a hydroelectric power or water supplier, may be interested in information on their reservoirs at resolutions less than 1 km. A sensor design must account for both the parameters it will measure and the spatial scale it will encompass.

The work outlined in this thesis is focused on current velocity measurement at ranges less than 3 km. This requirement defined the materials, assumptions, and principles used in its development. The fundamental parameter measured by the system is travel time of acoustic waves between two underwater locations. The average current velocity over the acoustic path is calculated using known formulas for the relationship between acoustic travel time and current velocity. Acoustic travel times also provide the ability to calculate temperature over the acoustic path. While the primary focus of the experiments is current, some temperature measurements are included.

The propagation of waves through a fluid medium is a function of many variables. The complex nature of travelling waves makes simulation very difficult and prone to inaccuracies if too many assumptions are used. Because of this, an experimental approach has been taken. Simplified formulae and models are used only as a qualitative confirmation of the experimental results. The primary objective of the thesis project was to design, build, deploy, and evaluate a system capable of using acoustic travel times to measure average current speed at scales less than 3 km. This experience is then used to provide design insights, quantitative limitations, and areas for continued focus in progressing this area of marine technology.

1.1 Problem Statement

Measuring current motion in large, open bodies of water presents many challenges. Flows can change direction and speed quickly across range, depth, and time. Currents observed in one area of a body of water may be very different from those in a neighbouring area, making

them difficult to track using single-point detectors. The instruments must also be deployed in harsh, unpredictable environments hindering longevity, reliability, and data accessibility.

The most common methods of underwater current detection each have their own benefits and pitfalls. Doppler-based instruments are very common and relatively inexpensive, but rely on signal scatterers to be present in the water which is not always the case [8]. Location based, free-drift, instruments do not require special instrumentation and can use the Global Positioning System (GPS) to track their motion [22]. However, with this technology it can take days to acquire a single current measurement. Satellite altimetry can provide unmatched spatial resolution but these systems are costly to deploy and require expensive satellite bandwidth.

Electromagnetic and mechanical methods are often utilized for measuring fluid flow through a pipe or narrow channel. Electromagnetic flow meters generate a magnetic field and measure its disruption when a conductive fluid flows through it. Mechanical methods include measuring rotations of a turbine driven by the fluid, and filling and releasing a chamber of known volume and counting the fills. Mechanical devices require a great deal of maintenance and can be difficult to use in environments with variable flow direction.

There are two commonly used forms of acoustic current measurement instruments - local point detectors with transducer separations of less than 1m, and purpose-built networks spanning large ocean distances. The precision required by the local instruments can result in issues when deploying in untested environments [27]. Further, the instruments are point detectors, and thus suffer from susceptibility to local flow anomalies. Large-scale, purpose-built networks have been utilized by oceanographers since the 1980s [18]. These can have separation distances between transducers that span entire oceans. Effects of current speed on travel time at these distances is quite significant making travel-time measurement precision less important.

It is conceivable that demand exists for a current measurement technique that provides real-time data for a small-scale ocean area. Such a product may be used as an additional tool to track iceberg paths near offshore oil platforms, to aid ocean cleanups, or to assist in searches covering large bodies of water. There is very little documented work on current averaging measurement instruments at this scale. Such a product would need to combine some of the precision of the point detectors with the synchronization methods used by large-scale oceanographic networks. This work attempts to address the need for a better understanding of the capabilities and limitations of such a system.

1.2 Contributions

This thesis documents the design, testing, and refinement of a cabled, short-range distributed network of acoustic transceivers. The system incorporates a novel combination of features including a power-over-data bus-link, high-efficiency Class D amplifiers, Modbus-based time synchronization and clock-drift correction, remote data collection for near real-time monitoring, and transmission-specific matched filter signal processing. An analysis of each design choice and its effect on system performance and accuracy is developed as a reference for future work in this area.

The experimental results included demonstrate the effect of the acoustic channel on controlled sound sources. This is another challenging subject area with respect to experimental data, as gathering such data requires construction of systems that can withstand the harsh environments. Two of the three documented experiments were performed outside in open water, providing results that cannot be obtained from the enclosed, reflective, environment of a tank. This information should provide guidance on the expected behaviour of acoustic waves and the limitations on travel-time measurement precision.

The included uncertainty analysis and lessons learned sections provide both a quantitative and qualitative analysis of the system. These results include clear areas for improvement and further development of such a system. It is anticipated that the major contribution of this work will be these results, which can be used as a guide for further research focused on the feasibility of a short-range, travel-time based, current monitoring network.

1.3 Organization

This thesis is broken down into five distinct sections as follows:

- Chapter 2 includes background information of ocean current measurement techniques. This includes an overview of the supporting physics, a brief history of travel time-based methods, a description of other methods, and an overview of some popular commercial products.
- Chapter 3 focuses on the system hardware. This section contains a complete system topology, discussion of the detailed design of system communications, power, and transducer interface circuits.
- Chapter 4 provides a description of the software used by the system. It includes descriptions of the programming techniques used in the distributed network of microcontrollers, data collection program, and digital signal processing.
- Chapter 5 presents the experimental results. Results of three distinct tests are included from various stages of system development. This section includes the objective, measurement data, and a system performance analysis from each test.
- Chapter 6 summarizes the system performance, a list of lessons learned, and recommendations for the focus of future work.

Chapter 2

Background

Research into the behaviour of acoustic waves has been undertaken for hundreds of years. The earliest records are of natural underwater seismic events that were observed to travel around the globe. In the early twentieth century man-made explosions were intentionally triggered and observed across oceans [14]. These events led to the important observation that acoustic waves travel relatively unimpeded through the water.

After several decades of experiments with explosive sources, enhancements in technology led to battery powered sources. Around the same time, underwater acoustic monitoring devices, hydrophones, were being researched heavily for surveillance purposes in World War 1 and 2. Much of the earliest research in this area is uncredited, as it was done in secret by military scientists.

By the 1970's global military research in this subject area had slowed considerably. However, ocean listening stations developed for submarine detection, such as the Sound Surveillance System in San Diego, were still active and available to researchers for the study of underwater sound. Portable battery and computer technology had also advanced to the point that measuring acoustic travel times had become more feasible. It was around this time that

Walter Munk and Carl Munsch first proposed the idea of measuring ocean temperature and current using the travel times of acoustic waves [15]. Munk and Munsch would go on to perform a considerable amount of research in that area over the next two decades. The bulk of the contributions from their publications was compiled into a textbook on the topic [14].

Much progress has been made in both ocean acoustic tomography and current measurement instruments, although ocean current remains an inherently difficult parameter to measure and working in the ocean environment comes with many challenges. These challenges mean there remains much to learn in this field.

2.1 Acoustic Wave Propagation in Water

The earliest records of observed long-distance acoustic wave propagations underwater were in the 19th century. Volcanic explosions were heard across the globe and some of strongest were shown to circumnavigate the globe multiple times before completely dissipating. In the first half of the twentieth century, and driven by World Wars I and II, underwater explosive testing in San Diego sent acoustic waves that were detected by military listening stations in Bermuda.

The expected Signal to Noise Ratio(SNR) of an acoustic wave at the receiver can be determined from the Sonar Equation[14]:

$$SNR = SL - TL - (NL - AG)\ dB \tag{2.1}$$

- SL: Transmission Signal Level (dB).
- TL: Transmission Loss (dB). Increases with range and frequency, this work assumes

a uniform spherical spreading loss of $20log(R)$, where R is the range from the transmitter.

- NL: Noise Level at the Receiver (dB). Decreases with frequency at the receiver as most sources of noise in the ocean are at low frequencies.
- AG: Array Gain (dB). If the receiver consists of an array of hydrophones the array gain is defined as the SNR improvement provided by combining the signals from the hydrophones.

As shown by the equation, the SNR at the receiver will decrease with range and increase with frequency. This makes it desirable to have the receiver and transmitter close together and to use high frequency transmission signals. In practice this is not always possible as a short range will limit the measurement area and higher frequency waves do not travel as far through the water.

In addition to level loss, the shape of the wave is also transformed by the acoustic channel as it travels. Acoustic waves dissipate through time and space in water, with the motion of the wave dictated by temperature, pressure, proximity to the bottom and surface, objects in the water, and the motion of the water itself (waves/currents). Sound in the water will bend away from regions of higher sound speed (higher temperature, higher pressure). This can create a "sound channel" or path that acoustic waves will want to follow between two points underwater. This axis is typically at about 1 km depth throughout most of the world's oceans. Reference [14] contains an appendix of sound axis graphs covering most of the globe.

As the wave travels parts of it will move through areas of differing pressure and temperature. This gives the impression at the receiver that the pulse has broken into multiple copies of itself. Some ray paths may interact with the surface or ocean bottom, changing their shape in complex ways. This means that a single pulse sent from a source will generate

many, sometimes heavily altered, pulses at the receiver. This phenomenon is called multipath propagation and is often modelled using ray theory [14].

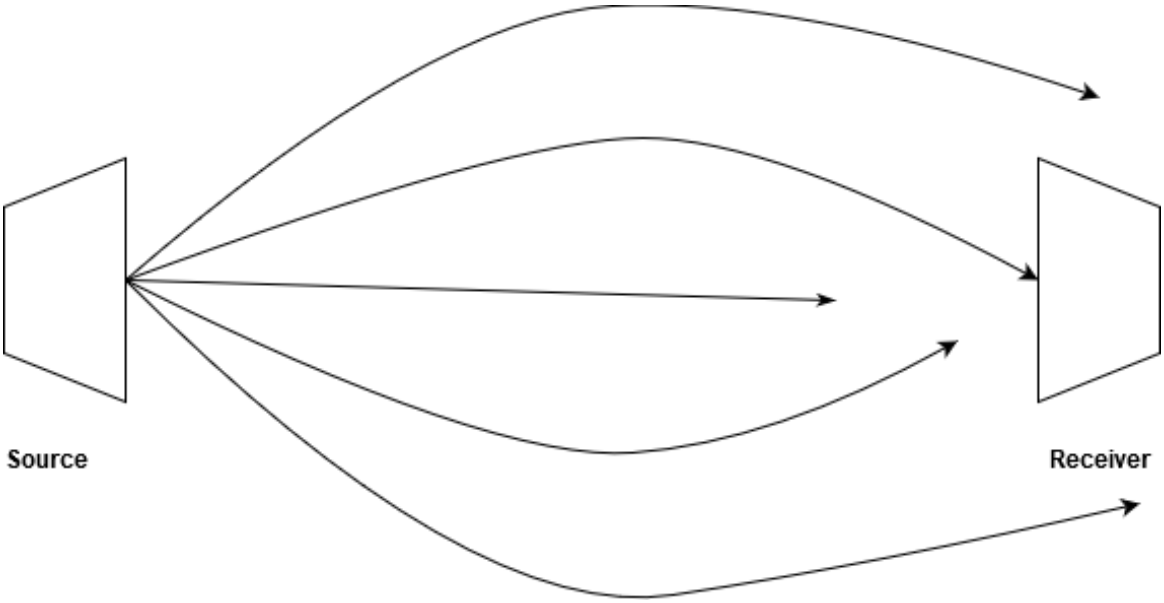

Figure 2.1: Visual Representation of the Multipath Effect

Although each source generates an infinite number of rays, only a finite number will intersect the transceiver. This can make the precise measurement of travel times difficult as a single pulse from the transmitter will appear as many pulses at the receiver. At large distances the different paths can be resolved more easily, while at smaller distances they often arrive as overlapping micro-paths. These micro-paths will sometimes interact destructively, cancelling the wave at the receiver.

While the system described in this work does not attempt to resolve ray paths, a brief description of ray paths is included as they are very evident in the testing data presented later. A great deal of literature is dedicated to resolving ray paths and inferring time spent at different depths to profile the water column. References [2], [9], [16], and [17] include just a small selection of the papers written on this topic.

There are several facts that are utilized in travel time-based temperature and current measuring systems:

- The acoustic pulses will travel faster in the direction of the water's motion.
- In a reciprocal transmission, acoustic rays will traverse the same path in both directions.
- Sound speed increases with temperature, salinity, and pressure.

Along with these facts, there are also some assumptions and simplifications used in this work:

- The motion of the water does not change between upstream and downstream acoustic transmissions. During testing, this duration was approximately 60 seconds.
- The motion of the water does not change by more than 50 cm/s between one set of upstream/downstream acoustic transmissions to the next. During testing, this was approximately 120 seconds.
- v_{water} as defined in the formulas is the average velocity of the water along the acoustic path. This work assumes that the path is axial and does not attempt to determine the bending radius, or resolve multiple ray paths.

These three facts and three assumptions were used to derive the following formulas for straight line sound propagation. These formulas are the basis for calculating physical parameters of current speed and temperature from the observed travel times. These formulas do not consider interaction with the surface, or bottom, bending, or other reflections.

1. The travel time in a single direction will include the water velocity component along with the sound speed:

$$v_{1,2} = c + v_{water} \tag{2.2}$$

2. Because the wave will traverse the same path in the opposite direction, the travel time in the opposite direction will include the same v_{water} component with the opposite sign.

$$v_{2,1} = c - v_{water} \tag{2.3}$$

3. By taking the average of the two travel times, you can isolate the sound speed:

$$v_{1,2} + v_{2,1} = 2c \tag{2.4}$$

4. The following formula defines the relationship between sound speed in water and the temperature, depth and salinity [13].

$$\begin{aligned} c =& 2.1 \times 10^{-4} T^3 \\ &+ \left(-5.44 \times 10^{-2} + 8.7 \times 10^{-5} S + 3 \times 10^{-7} Z\right) T^2 \\ &+ \left(5 - 1.23 \times 10^{-2} S - 9.5 \times 10^{-13} Z^3\right) T \\ &+ 1402.5 + 1.33 S + 1.56 \times 10^{-2} Z + 2.55 \times 10^{-7} Z^2 \\ &- 7.3 \times 10^{-12} Z^3 + 1.2 \times 10^{-6} Z(\Phi - 45) + 1.43 \times 10^{-5} SZ \end{aligned} \tag{2.5}$$

As is evident from the equation, the greatest dependency is on temperature. If the pressure and salinity along the acoustic path are known, this formula can be used to calculate the water temperature along the acoustic path. Temperature, salinity, and depth can be measured at the node points using commonly available CTD instruments.

By subtracting the travel times of the acoustic waves in opposite direction, the v_{water} component can be isolated and the current along the acoustic path can be measured.

$$v_{1,2} - v_{2,1} = 2v_{water} \tag{2.6}$$

Together, these formulas form a set of equations and unknowns. In a scientific or commercial deployment neither the distance, temperature, pressure, acoustic path, or salinity will be precisely known. The temperature, pressure, and salinity could be measured at the nodes with a CTD instrument. The acoustic path can be determined by resolving a set of travel times and defining the path for each ray accordingly.

2.2 History of Acoustic Travel Time Current Sensing

The first recorded instance of using reciprocal travel times to measure currents in the ocean is from 1976 [14]. Two transceivers suspended from ships 25 km apart were used to send reciprocal transmissions. Fourteen ray paths were successfully tracked and the reciprocal travel times of each were measured. This experiment proved that measuring ocean currents at the mesoscale was possible and paved the way for future projects and refinements in the area.

The same group continued experiments throughout the 1980s and 1990s. The focus of their work was on large-scale oceanography, and with each project the mapping area became larger. Much of the literature from this period is dedicated to the interpretation of multiple ray path travel times over large distances. This work has been the basis for many ocean-wide (basin-scale) experiments since that time.

Reference [3] contains an extensive investigation into the notable tomography experiments of the 1990s. The experiments cover locations all over the globe such as the Greenland Sea, the Strait of Gibraltar, and the Arctic Ocean. Some experiments were fixed systems with cabled or satellite communication streaming the data to land and others were temporary experiments with store-and-retrieve data collection methods. These experiments were conducted over large areas of ocean with a focus on determining shifts in ocean currents and associated effects on the global climate. The paper [3] claims that acoustic tomography methods are not suitable for shallow water because of interaction with the bottom and surface.

Throughout the 1990s and 2000s two other methods of ocean current sensing were evolving. Satellite altimetry, which uses the reflection of electromagnetic waves, and drift methods, which let instruments drift with the currents at different depths and then report their locations. Reference [4] proposes that the future of ocean tomography is to act as a complement to these methods. The Argo project outlined in [22] is a network of floats which, at the time of this writing, comprises a network of 3,868 floats. Satellite altimetry systems operate along most populated coastal areas and can provide current speed measurements for shallow oceans but cannot penetrate to the deep ocean. Acoustic tomography can be used to bolster this data and can provide data on less-understood ocean processes such as vorticity and convection [3].

As processing power and data storage becomes more accessible, numerical models of the ocean are becoming more accurate. These models require data from all sources for verification, prediction, and refinement. Reference [4] concludes that these models would benefit greatly from more acoustic tomography data, although there is little work being done in this area. In all cases, the work is focused on large-scale ocean studies.

In the past decade, a group in Japan has done several experiments on short range acoustic travel time based current measurements. They have deployed sets of transceivers across rivers and calculated the volumetric flows based on the differential travel times. [1] describes one of their experiments across a 30km range. [11] demonstrates the expansion of the idea into tomography networks in which two pairs of transducers measure current vectors and the flow direction is calculated from their intersection angle. A number of this groups' papers, [12] and [21], use methods developed in oceanography to approximate the ray path based on the travel times and use these to infer water flow at various depths. Their work is closely related to the work in this thesis, with the primary differences being their focus on river applications and their use of GPS time synchronization between unconnected nodes.

Another class of acoustic travel time current sensing are localized point detectors. References [5] and [6] describe a 3-dimensional acoustic travel-time current point-detector from Falmouth Scientific Inc. Reference [25] describes the development of the MAVS3 (Modular Acoustic Velocity Sensor), another acoustic travel time point detector. These devices use sets of transducers mounted on a single frame to measure reciprocal travel times over distances of a few centimetres. These devices only measure the travel time across the short (approximately one metre) separation between their transducers, hence, the devices only measure current and temperature at their location.

2.3 Other Current Sensing Methods

The most commonly used current sensing instruments rely on the Doppler effect. Acoustic Doppler Current Profilers (ADCPs) send acoustic pulses and measure reflections from nearby particles moving with the current. The Doppler effect states that the frequency of the reflections will be proportional water velocity component in the direction of the acoustic

source. These devices can provide vertical and horizontal current profiles in the hundreds of metres range. They require reflective particles to be in the water and are highly sensitive to noise and reflective surfaces near the transducer.

Drifting devices are capable of measuring currents over wider areas. Drifting device methods involve an instrument that follows a report-dive-drift-surface-report sequence. One of the most prominent examples of these types of devices are those used in the Argo project. As previously discussed, the Argo project is a massive network of drifting instruments. The instruments report periodically on ocean temperature, salinity, and current speed. Data from the Argos is used by oceanographers, researchers, and modellers around the globe.

Satellite altimetry is another method of measuring current and temperature over wide ocean areas. Satellite systems send high-frequency electromagnetic waves toward the ocean surface and study the reflections and back-scatter to infer information about the ocean. These systems are used by researchers as well and have also found uses in meteorology and marine reporting.

X-Band radar methods utilize shipboard radar systems, originally intended for navigation, to measure ocean currents. The back-scatter of the radar pulses are analysed to determine properties of the sea state. Reference [7] is a recent paper on this topic that includes a comparison to ADCP data with favourable results.

There are many other methods in use to measure ocean currents. Mechanical current meters have many forms and have been used for hundreds of years. There are other varieties of electromagnetic-based current measurement schemes. Ocean density measurements can be used to calculate current speed as well.

There are pros and cons associated with each of these methods. ADCPs can provide high-resolution vertical and horizontal profiles but their accuracy is very sensitive to obstructions in the water or on the surface. Drifting devices have range-averaging noise reduction but

can take days to obtain a single measurement. Satellite altimetry can provide high resolution current maps in depth and range but are expensive to build, deploy, and maintain. X-band radar methods use instruments that have been in use for many years for ship navigation, but require reflective particles and have limited range. Mechanical devices use simple, proven, methods but the moving parts are prone to failure in marine environments.

2.4 Commercially Available Acoustic Travel Time Devices

There are presently no commercially available products that measure currents with differential travel times over wide areas. There are two classes of products in existence - travel-time based point detectors and custom-built transducer arrays. Two commercially available travel-time based current detectors are the Falmouth Scientific ACM Plus [5], [6] and the Nobska Development Corporation MAVS3 [25], [28], [27], and [19]. Each of these products compete with the more commonly used ADCP type instruments.

Wide area transducer arrays for measuring current are deployed around the globe. At least two United States patents have been issued for such systems [24], [10] although there is no indication that these have been developed into commercial products. These arrays are typically custom-built for research projects by a University, government, or military organization. There is very little record of any type of differential travel-time based current measurement system used in the 100m to 3km range that is the focus of this research. Many papers claim that micro-paths, surface/bottom interaction, and the need for precise timing measurements prevent this method from being feasible at these ranges [3].

Chapter 3

Hardware

The hardware of the system is the basis for meeting the basic requirement of accurately measuring acoustic travel times. The hardware design included microcontroller selection, circuit design, and subsea cable splicing. The following specifications define the hardware design:

1. The system must contain two underwater nodes.
2. The system must be capable of running autonomously for one tidal cycle.
3. The system must be powered from a single 12VDC power supply.
4. Each node must be powered through a shore cable.
5. The nodes must communicate with a shore station to send acoustic data.
6. The shore cable will contain only two conductors.
7. Each node must be capable of transmitting and receiving acoustic waves across distances of up to 150m.
8. Hardware-induced measurement delays must be close enough in both nodes so that differential travel times can be measured to an accuracy of $\pm 5 \mu s$.

9. The nodes and subsea cables must operate fully submerged at depths up to 10m.

10. Each nodes must be able to transmit acoustic waves and record them simultaneously.

This set of requirements was developed with consideration of the testing of such as a system. The goal was to develop a two-node system that could be deployed in a tidal channel for one tidal cycle. Some requirements were also driven by equipment availability as all equipment used for the project was repurposed. Part of the investigation, and value in this work, is the ability to compensate for hardware deficiencies with novel software and data-processing techniques.

3.1 Topology

The system topology in a typical deployment is shown in Fig. 3.1. The shore station is positioned close to the water and connected to a data collection PC, a DC power supply, and the two remote nodes via the shore cable. The shore cable is connected in a daisy-chain configuration to the two subsea nodes. Each node is contained in a watertight enclosure and is connected to a hydrophone along and the shore cable.

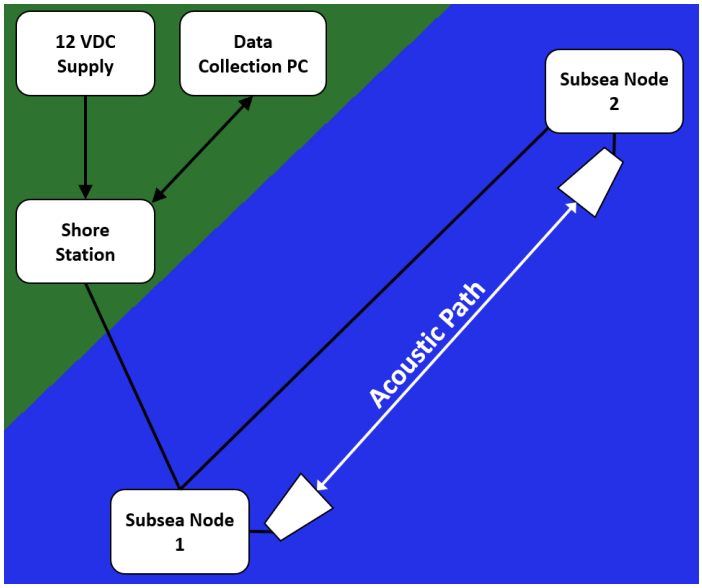

Figure 3.1: System Topology

Each subsea node contains three main components:

- Arduino UNO microcontroller.
- Hydrophone interface circuit.
- Power/data decoding and encoding circuit.

The shore station also contains three main components:

- Arduino MEGA microcontroller with SD Card interface.
- Power/data decoding and encoding circuit.
- User control switches for powering and running the system.

The following diagram shows a block level view of the circuitry in the shore station and connections to the shore cable. Subsequent sections will provide greater detail with respect to the design of each circuit.

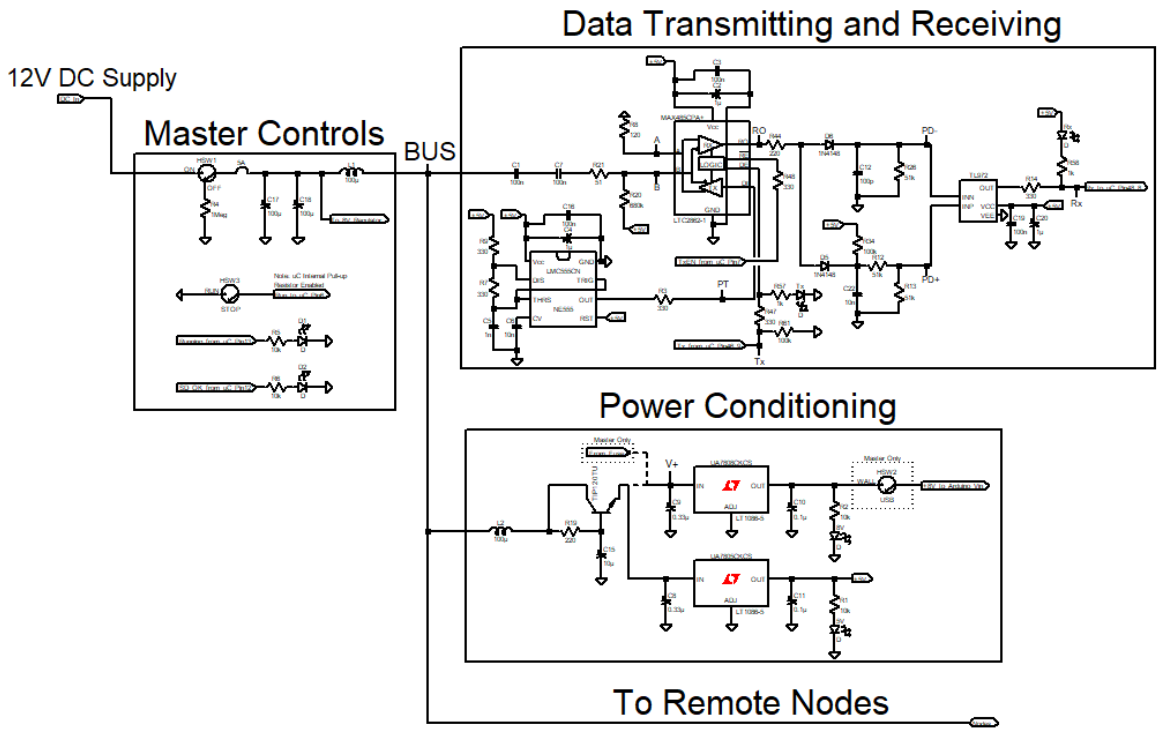

Figure 3.2: Inter-node Power/Data Bus from Master's Point-of-View

The shore cable contains only two conductors with the data superimposed on top of the 12VDC supply to the subsea nodes. Fig. 3.3 shows a waveform capture of a data packet being sent on the shore cable. The data packets consist of 5V pulses centred around a 12VDC offset.

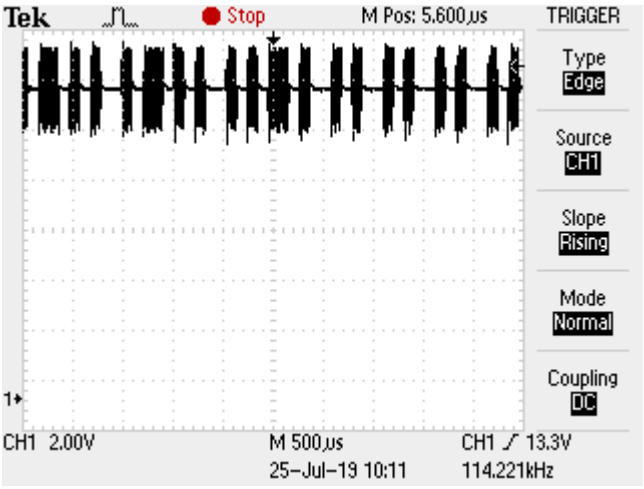

Figure 3.3: Waveform Capture of the Power/Data Bus (Fig. 3.2 Ch.1: *BUS*)

3.2 Power

The system operates on a single-sided 12VDC supply. This supply is connected at the shore station and sent to the subsea nodes via the shore cable. The master and the nodes contain 8V and 5V regulators for stepping down the supply for powering the Arduinos and integrated circuits, respectively. The 12V supply line is supplied directly to the signal transformer during hydrophone transmissions to allow for maximum supply current to the amplifiers.

As the shore cable contains only two conductors, this system uses a power-over-data design. This creates the need to filter the incoming feed from the shore cable before passing the DC voltage to the devices. The power filtering circuit consists of an inductor in series with a capacitance multiplier. The inductor acts as a high impedance at higher frequencies. The capacitance multiplier provides further ripple protection by acting as a very large capacitor to ground at the DC input of each node. The power conditioning circuit is shown in Fig. 3.4.

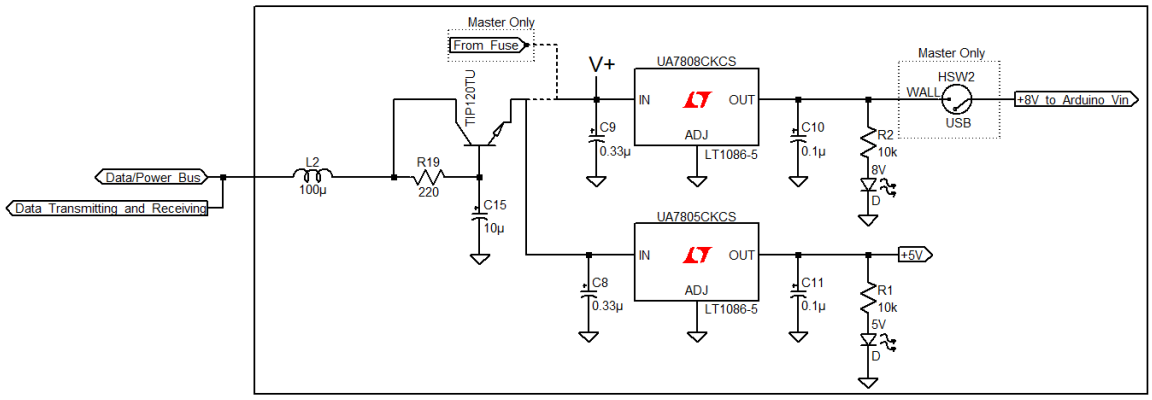

Figure 3.4: Power Conditioning Circuit

Fig. 3.5 shows a waveform capture of the incoming supply after filtering of the data packets. The ripple was reduced to 200mV pulses under full load after filtering, or 4% of the original data pulses. It should be noted that the ripple reduction provided by the circuit is inversely proportional to the loading of the supply and thus may not be effective for larger networks.

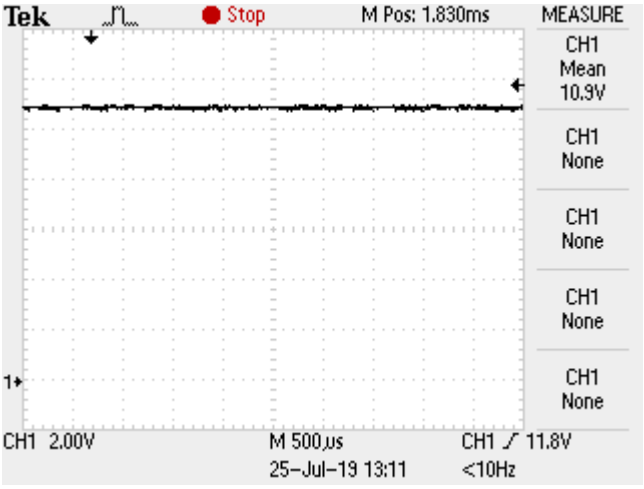

Figure 3.5: Power Supply After Filtering (Fig. 3.4 Ch.1: $V+$)

3.3 Microcontrollers

The microcontrollers used are Arduino UNOs in the subsea nodes and an Arduino MEGA in the shore station. Arduinos have the advantage of being easy to program, well documented, and supported by a large online community.

The Arduino uses a 16 MHz clock and a 10-bit Analog to Digital Converter (ADC). These limitations created the need for efficient data capture and storage methods. As this is a timing-critical application, all unnecessary processes are stopped on the microcontrollers when a data capture event is happening to prevent delays in reading the ADC. Only the most significant 8 bits of the 10-bit ADC are stored to increase the rate of data capture and sample duration.

The Arduino UNO has 32kB of combined program and data space. The size of the program was kept to a minimum to allow maximum space for data during a capture event. The limit was reached at the storage of 850 8-bit samples. The sample rate is 76, 942 Hz, therefore the system is capable of capturing hydrophone samples 11ms in duration before needing to

send the data to the shore station. The acoustic frequency of the system is adjustable but the testing data used a frequency of 12.5 kHz, thus it is sampled at approximately 3 times the Nyquist rate.

3.4 Communications

The communications circuitry is identical in the shore stations and subsea nodes. It consists of a data decoder for de-coupling received data from the 12VDC supply and an encoder for super-imposing transmissions onto the line. Fig. 3.6 shows the data decoding/encoding circuit. This circuit was adapted from the design found at [26].

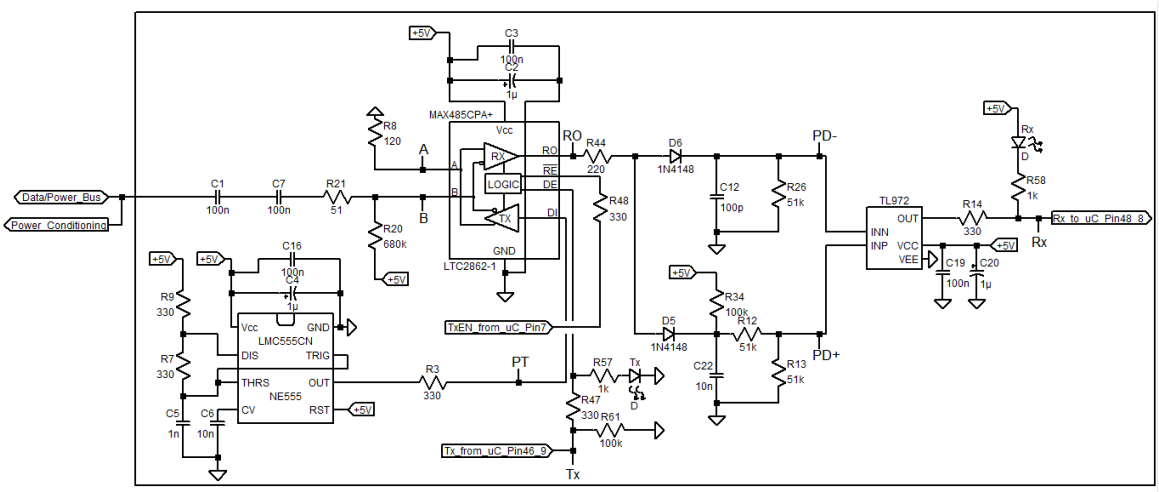

Figure 3.6: Data Transmitting and Receiving Circuit

The network uses the Modbus communications protocol. At 9600 bps, the data transmit rate is approximately 10 kHz. The filters in the power circuit would not show a high enough impedance at this frequency and so the data is modulated to 1MHz. This modulation is achieved by connecting a 1 MHz pulse train into the MAX485 data input and connecting the Modbus transmit from the microcontroller to the data enable pin. The modulation also prevents long strings of 1's in the data from appearing as a DC voltage and being dropped by

the coupling capacitors. Fig. 3.7 shows this modulation.

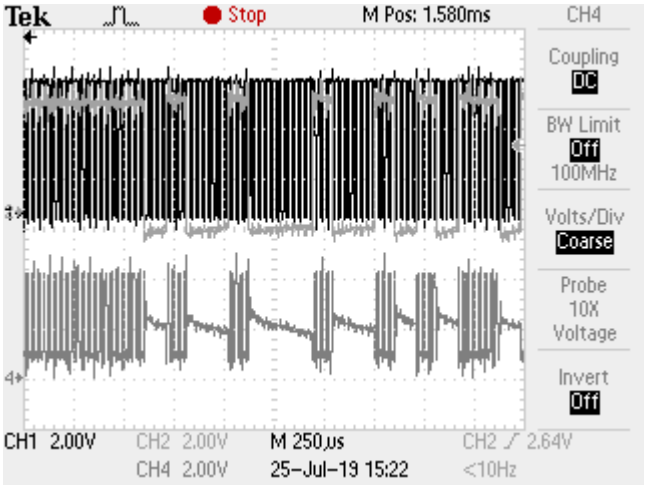

Figure 3.7: Modulating Outgoing Modbus Transmissions (Fig. 3.6 Ch.1: PT, Ch.2: Tx, Ch.4: B)

The received data is fed through a coupling capacitor to remove the 12V DC component. The zero-mean data is then buffered via the input of the MAX485 chip. This buffering creates a predictable impedance on the shore cable and allows the input data to be shifted up to 0-5V. The timing of the Modbus data is recovered with a peak detector circuit tuned to operate in the range of the expected data rates. The timing recovered signals are then buffered again via a 5V op-amp comparator before connecting to the receive pin of the microcontroller. Fig. 3.8 and Fig. 3.9 show a de-coupled incoming transmission and timing recovery respectively.

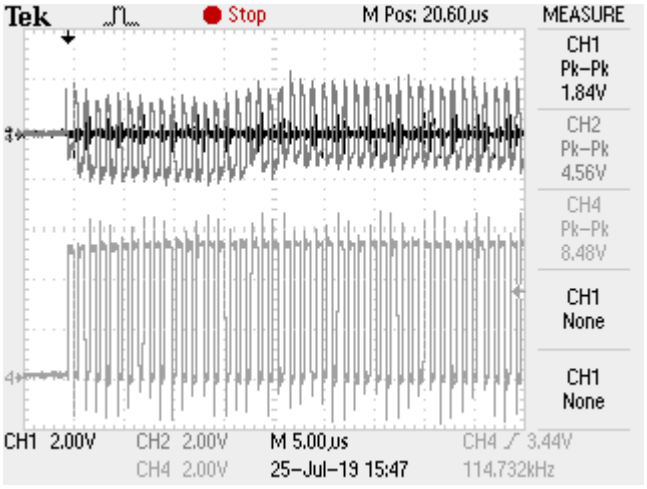

Figure 3.8: Buffering Received RS485 Data (Fig. 3.6 Ch.1: *A*, Ch.2: *B*, Ch.4: *RO*)

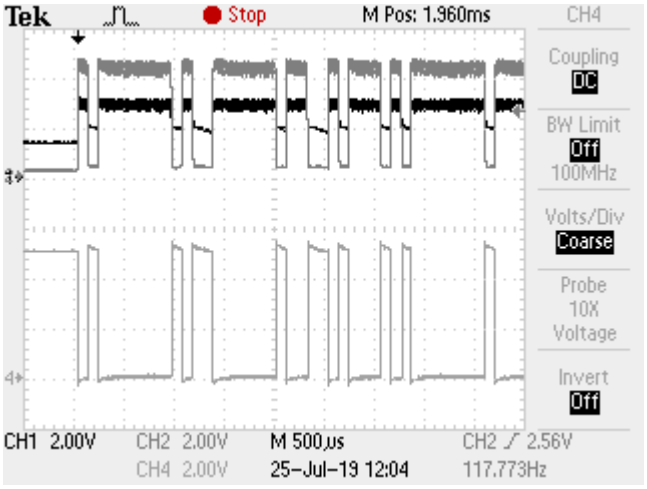

Figure 3.9: Timing Recovery of RS485 Data (Fig. 3.6 Ch.1: *PD+*, Ch.2: *PD−*, Ch.4: *Rx*)

3.5 Hydrophone Interfaces

Each subsea node is connected to an acoustic transducer (hydrophone). The hydrophone is capable of acting as transmitter or receiver. The hydrophone interface circuitry contains two distinct paths which can be switched via a Single-Pole-Double-Throw relay controlled by the microcontroller. As receivers, the hydrophones used have a peak response around 12.5kHz.

As such, that frequency was chosen for the acoustic transmissions, though the frequency and transmission codes can be modified from the shore station during operation as each individual transmission is read-back for the matched filter calculations. These aspects are discussed further in the software section.

The transmitter circuit must achieve sufficiently high voltage levels to overcome spherical spreading, the noise in the receiver amplification circuit, and the in-band ambient noise in the area. The required amplification and signal shape is achieved by a Class D amplifier and small signal output transformer. Fig. 3.10 shows the hydrophone transmission amplifier.

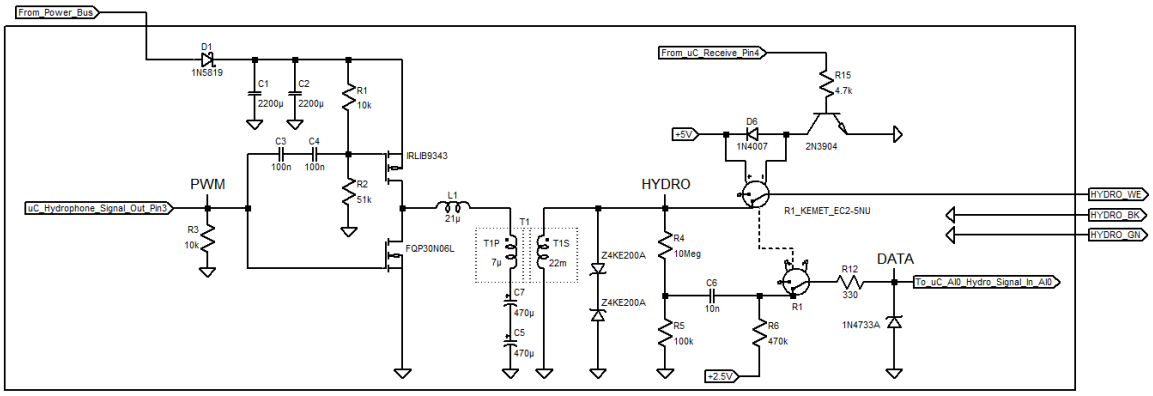

Figure 3.10: Hydrophone Transmitting Circuit

The microcontroller sends a 0-5V Pulse Width Modulated (PWM) signal to the amplifier (Fig. 3.11). This signal is relayed directly from the 12V supply and sent through a low-pass LC filter connected to the output transformer. The output transformer converts the 0-12V sine wave into a -200-200V sine wave (Fig. 3.12). The transformer secondary is connected directly to the hydrophone and generates acoustic pulses that can easily be heard 150m away.

The PWM signal from the microcontroller varied from 50kHz to 250kHz and the LC filter provided a cut-off frequency of 1.5kHz. This provided sufficient filtering to supply a smooth 12.5kHz sinusoid to the transmitting hydrophone as can be seen in the figures.

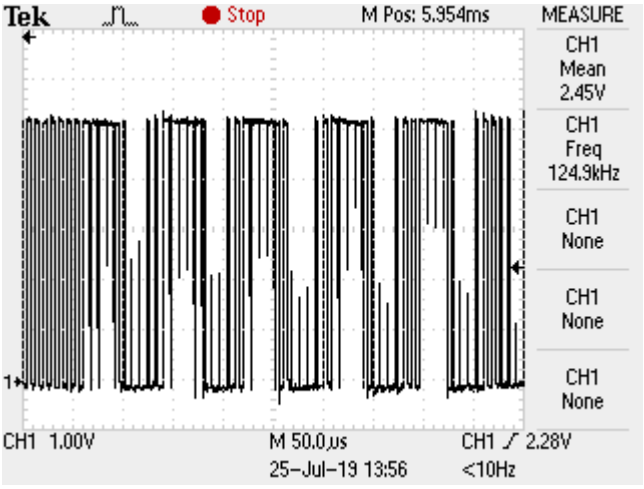

Figure 3.11: PWM Signal from Microcontroller (Fig. 3.10 Ch.1: PWM)

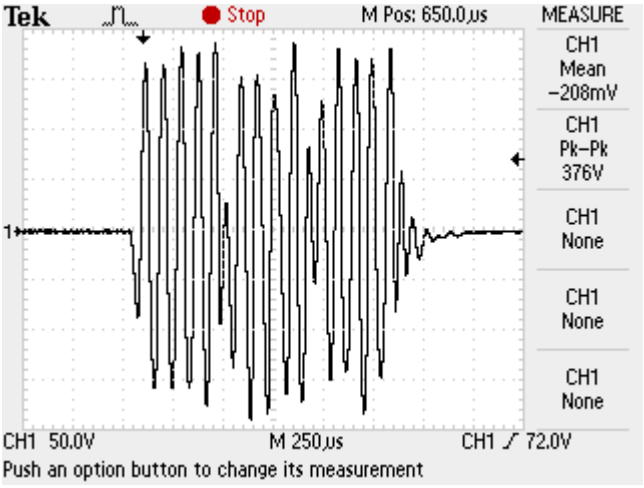

Figure 3.12: High Voltage Signal to Hydrophone (Fig. 3.10 Ch.1: $HYDRO$, R1 De-energized)

The transmission circuit also contains a feedback into the microcontroller's ADC. The signal going to the hydrophone is attenuated and shifted to connect to the ADC. This allows each transmission to be captured and used in the matched filter process to determine the travel time. It also allows the user to try different waveforms on-the-fly without having to reconfigure a sample waveform. It captures any distortions and timing delays introduced by the amplifier for each individual transmission. Fig.3.13 shows a read-back signal. It should be noted that this scheme does not capture distortions or delays introduced by the transducer.

However, there is strong correlation between the read-back and received signals evident in the testing data.

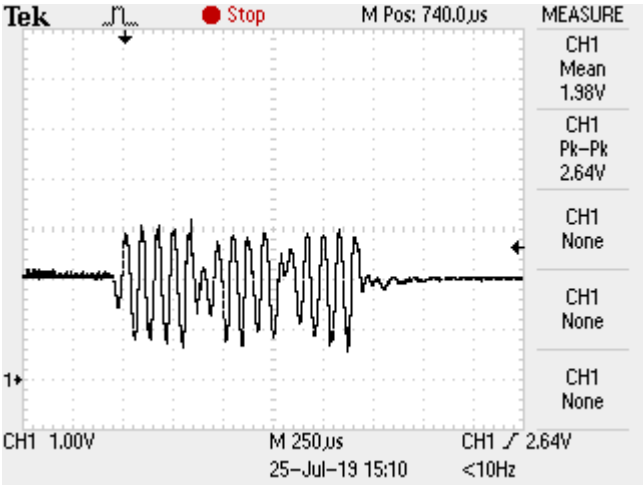

Figure 3.13: Attenuated Read-back Signal (Fig. 3.10 Ch.1: *DATA*, R1 De-energized)

The receiving circuit is shown in Fig. 3.14. It consists of a two-stage amplifier with voltage-controlled gain. The first stage is a charge mode amplifier typically used for hydrophones. This stage presents a very high impedance to the hydrophone. The next stage is an op-amp based inverting amplifier with voltage-controlled gain [26]. This allows the user to control the gain of the receiver for use in different environments. Hydrophone waveforms before and after amplification are shown in Fig. 3.15 and Fig. 3.16 respectively.

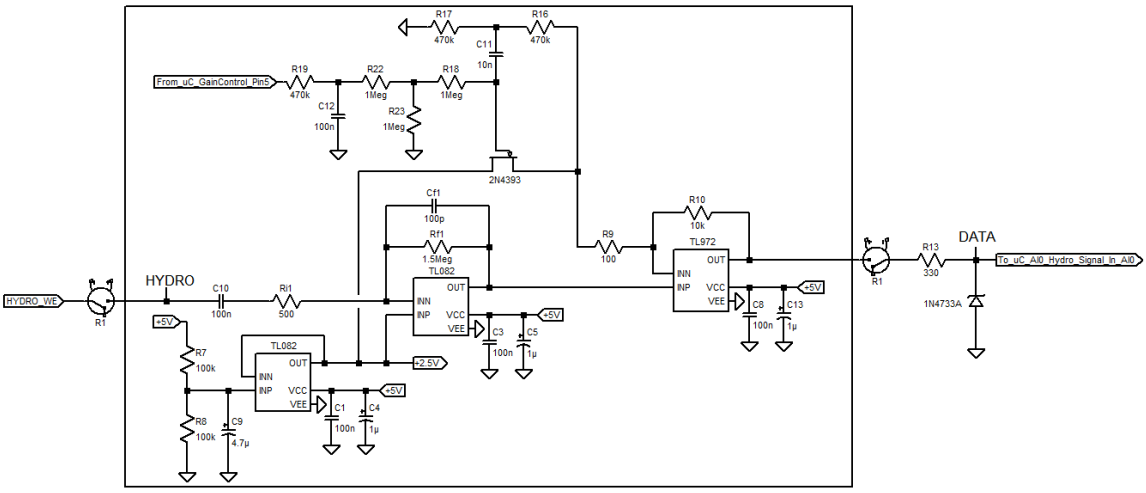

Figure 3.14: Hydrophone Receiving Circuit

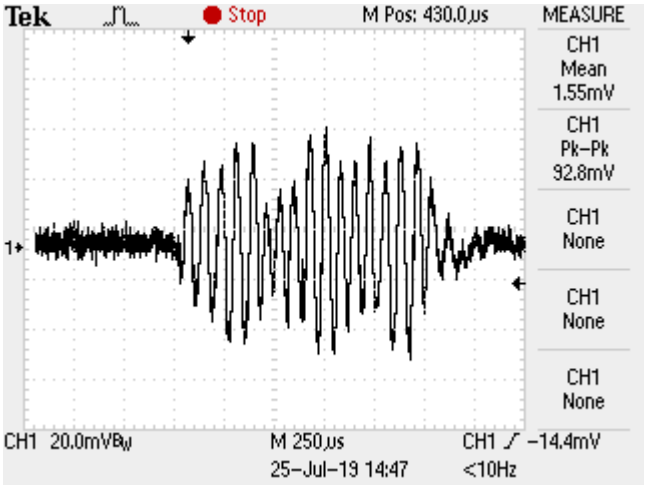

Figure 3.15: Signal Received from Hydrophone (Fig. 3.14 Ch.1: *HYDRO*, R1 Energized)

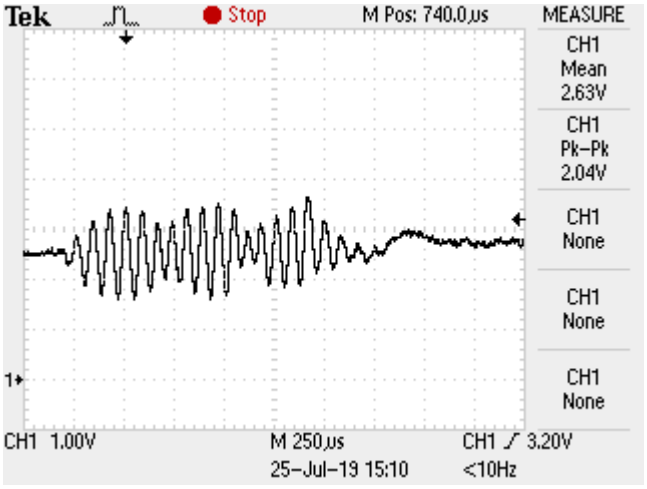

Figure 3.16: Amplified Signal from Hydrophone (Fig. 3.14 Ch.1: *DATA*, R1 Energized)

Chapter 4

Software

The software package for the system consists of three major components. A microcontroller program written in C runs on the underwater and master nodes. This program handles data collection, pulse triggering, and sequence control. There is a C-based computer program that runs on the data collection computer, it handles serial communications with the master controller. This program receives the data stream and sends user commands to the master node. A MATLAB program is used to visualize and process the raw data into travel times and physical measurements.

A set of requirements for each piece of software was developed. Project goals, testing plans, and equipment availability drove these requirements.

The Arduino programs requirements were as follows:

1. The subsea node software must require less than 32kB of space (the size of the Arduino UNO program space).
2. The master node must require less than 256kB of space (the size of the Arduino MEGA program space).

3. Must be able to capture and store 10ms of hydrophone data at a sample-rate of 25 kHz or higher.
4. Must be able to synchronize subsea node clocks using only a Modbus message from the master.
5. Must be able to send the data back to the shore station after a capture from the hydrophone.
6. Transmission sequences and acoustic frequency must be able to be changed via a command from the user when the system is deployed.
7. Must be able to measure clock drift between subsea nodes.
8. Must run autonomously for one tidal cycle.

The C-based data capture program on the laptop is driven by these requirements:

1. Must be able to capture data from the onshore master via the USB port.
2. Must capture all data from the master and store it in a format that can be parsed by the MATLAB data processing code.
3. Must be able to transmit commands from the user to the master and subsea nodes while the system is deployed.

The MATLAB code for processing of the data onshore has the following set of requirements:

1. Must adjust the timing and sample rate of the received waveforms based on the measured clock drift.
2. Must be able to measure the travel time of an acoustic wave based on a transmitted and received waveform.

3. Must provide effective visualization of the transmitted and received waveforms to the user.

4. Must be able to process a large volume of travel times into temperature and current trends.

5. Must be able to calculate travel times from noisy data with heavy multipath interference.

These requirements drove the development of the three pieces of software required by the project. The following provides an in-depth discussion of the different software components.

4.1 Measurement Sequence

The network operates on the principal of command and response between the onshore master and the two underwater nodes. The master initiates the transmission sequence by assigning roles to the nodes - one node is always the transmitter and the other is the receiver. Both the master and node flow sequences can be represented in state transition diagrams as shown in Fig. 4.1 and Fig. 4.2.

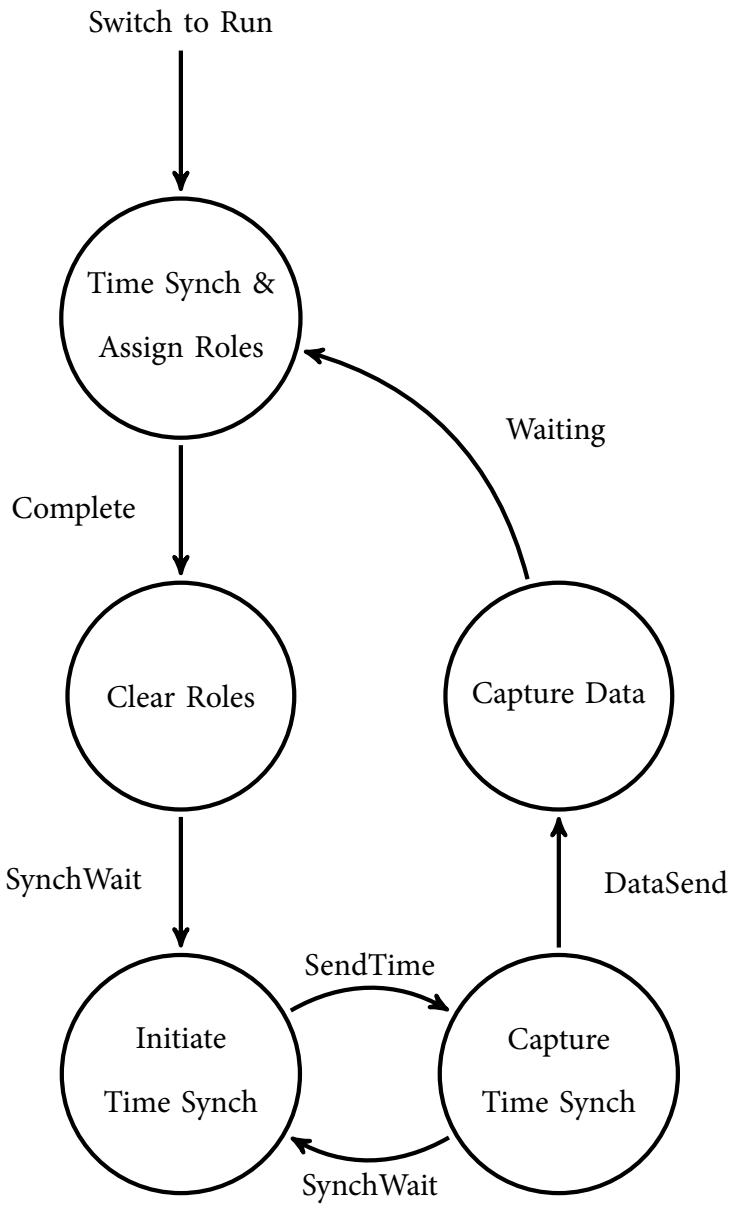

Figure 4.1: Onshore Master State Transition Diagram

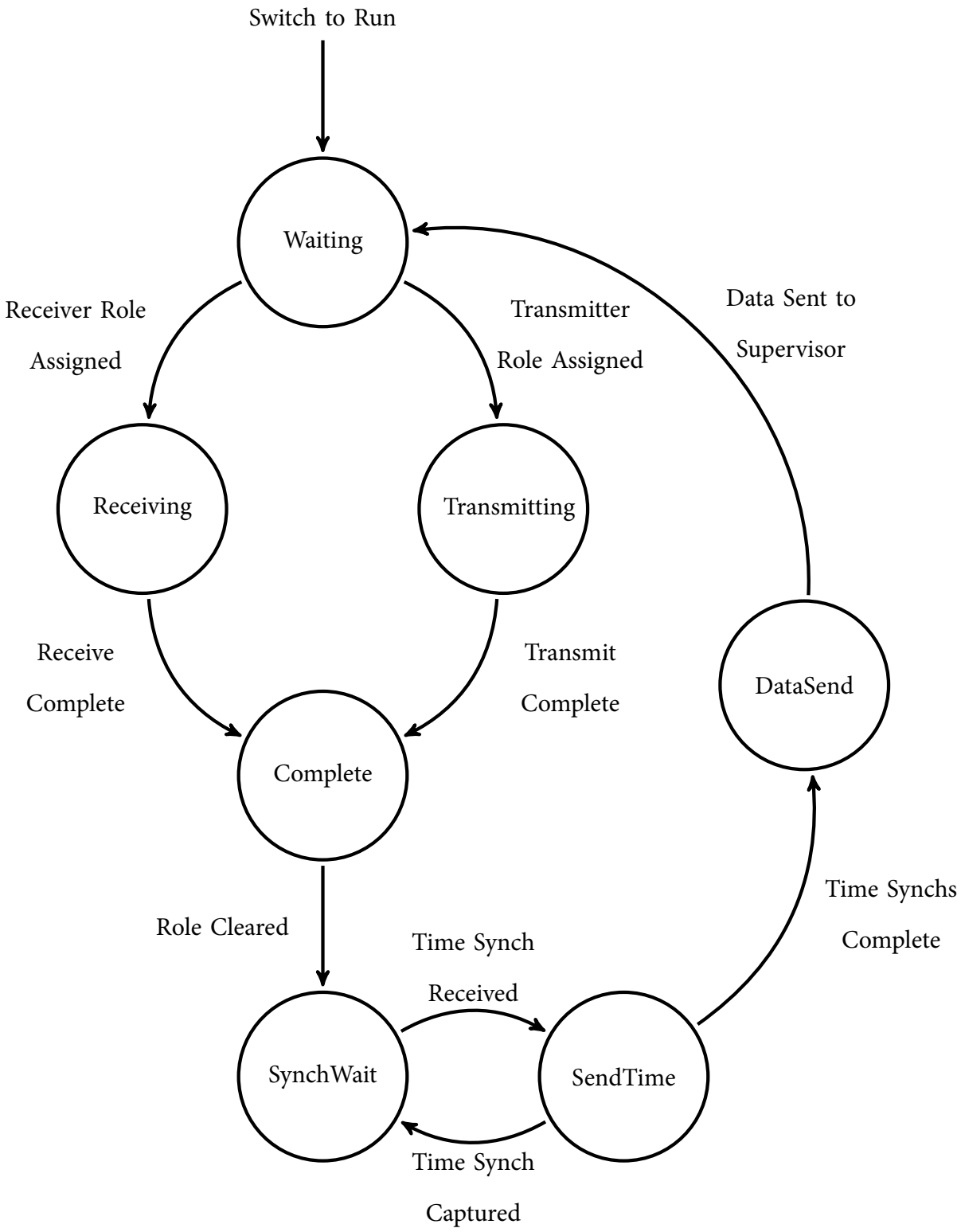

Figure 4.2: Subsea Node State Transition Diagram

The design is based on minimum control theory. The master node sends the minimum commands required to keep the system synchronized, allowing the nodes to perform their receipt and transmission stages without interference. After being assigned their roles by the master both nodes disable their Modbus communications and operate independently. The transmitter waits for a configurable delay and begins sending the PWM signal to the amplifier while recording the output signal back and storing it. The receiving node waits for the configurable expected time of arrival, it then records approximately 10ms of hydrophone data and stores it. During this time all resources of the microcontrollers are dedicated to wave generation, sampling, and recording.

The nodes re-establish communications with the master upon completion of the transmission and receiving phases. The network enters into a time synchronization cycle when the master sends periodic pulses to the nodes and the nodes record the arrival times. Further discussion is provided in Section 4.2. The last phase of the cycle is data collection. In this phase each node sends its hydrophone samples, time of last sample, and recorded times of synchronization pulses. This data is received at the onshore master unit and stored on a local SD card to be processed later.

4.2 Time Synchronization

Time synchronization was one of the biggest challenges during development. The requirement to be able to operate at short-range node separation distances means that the relative clock-drift between the underwater nodes must be accurately measured. The single conductor pair in the shore cable prevented a dedicated wired link for sending pulses. The nodes were not wired to the surface and so GPS time synchronization was not possible.

A Modbus register is used to achieve a time synch command. The master writes an integer into the top Modbus register and broadcasts it on the network. The Modbus interrupt on each node is programmed to check for the sequence of bits in this integer and store its clock value at the time of receipt of the final bit. This bit will be received simultaneously at each node, except for a propagation delay of 4 μs (measured) at the more distant node.

When responding to the Master, each node sends the time of last sample along with its data as discussed in Section 4.1. The time reported by each node is the clock value at the final recorded sample minus the clock value at the instance of receiving the time synch pulse. As each node samples at a constant rate, the time of last sample can be used to assign a time to each sample and build the time series for the data.

It was discovered early in testing that the clock drift between different Arduinos was more than sufficient to cause unacceptable error in the received times. Drift rates of up to 1us/ms were observed between two controllers. As the system requires a 500ms setup time after synchronization, at a 100ms travel time the clocks may have drifted by as much as 600 μs in this time.

Fig. 4.3 shows measured clock drift from a field sample. The horizontal axis is the ms counter of the master node, the blue line is the ms counter in Node 1, and the red line is the ms counter in Node 2. In the figure on the left it appears that the counters are all at the same value, but a zoomed in view of the 600ms point shows the approximate 600 μs difference in the counters of nodes 1 and 2. This would translate to an error of almost 450 cm/s in a current measurement over a 150m range.

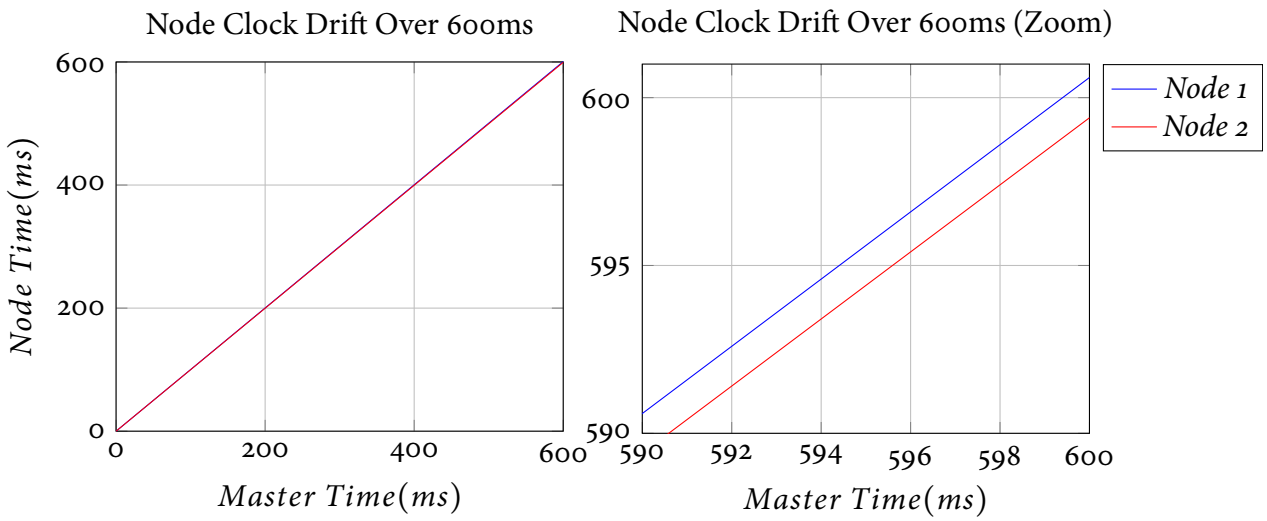

Figure 4.3: Clock Drift Over a 600ms Time-span

This amount of drift was unacceptable and required correction. The high-precision requirement and unpredictable deployment environment presented challenges in applying this correction. Attempts at pre-deployment calibrations were unsuccessful as the clock drift would swing with variation in the ambient temperature of the deployment environment. At these precision levels, other variables such as relative humidity, controller age, and running time would also throw off static calibration offsets.

For this reason, it was decided to measure the relative node clock drift during each sample sequence. To achieve this, the master sends a series of periodic time synch pulses and each node records the time of receipt of each pulse. The mathematical determination of clock drift based on the returned values are described next.

This section utilizes a unique set of symbols defined below:

- $\tau_{i,j}$: The time reported by node i of the arrival of time synchronization message j.
- $t_{i,j}$: The actual time node i received time synchronization message j.
- δ_i: The fraction that node i's clock has drifted from an ideal $16MHz$.

- $t_{prop,i}$: The propagation delay of the time synchronization message from the Master to node i.

The following equation relates the times reported by the nodes (the τ's) to the true times (the t's).

$$\tau_{1,1} = \delta_1(t_{1,1} + t_{prop,1}) \qquad \tau_{2,1} = \delta_2(t_{2,1} + t_{prop,2}) \tag{4.1}$$

Both clocks have independent drift errors and propagation times. However, for determination of the differential travel time, only the relative clock drift between the two nodes is required. The difference in propagation times to node 1 and 2 is what is required. The propagation time to node 1 can be set to 0 and a new variable can be defined that represents the propagation time from node 1 to node 2.

$$t_{prop,2,1} = t_{prop,2} - t_{prop,1} \tag{4.2}$$

The time-scale can now be adjusted from being relative to the master node, to being relative to node 1 by setting $\delta_1 = 1$ and $t_{prop,1} = 0$, and the equations become:

$$\tau_{1,1} = t_{1,1} \qquad \tau_{2,1} = \delta_2(t_{2,1} + t_{prop,2,1}) \tag{4.3}$$

Once the first time synchronization message has been received, $\tau_{1,1}$ and $\tau_{2,1}$ are sent to the master to be recorded. After this, a second time synchronization message is sent to the

nodes. Defining $\Delta t_{1,2}$ as the time between the two pulses, the nodes will report the following receipt times:

$$\tau_{1,2} = t_{1,1} + \Delta t_{1,2} \qquad \tau_{2,2} = \delta_2\left(t_{2,1} + t_{prop,2,1} + \Delta t_{1,2}\right) \tag{4.4}$$

Subtracting the equations in 4.3 from the equations in 4.4 results in the following equations:

$$\Delta t_{1,2} = \tau_{1,2} - \tau_{1,1} \qquad \Delta t_{1,2} = \frac{\tau_{2,2} - \tau_{1,2}}{\delta_2} \tag{4.5}$$

Setting the two equations in 4.5 and rearranging gives the following:

$$\delta_2 = \frac{\tau_{2,2} - \tau_{2,1}}{\tau_{1,2} - \tau_{1,1}} \tag{4.6}$$

As all of the τ values are known, the difference in clock rates between the two nodes (δ_2) can be calculated and used to adjust the time scale of the higher designated node.As $t_{prop,2,1}$ is a constant it was measured in the lab to be 4.0 μs and numerically applied during current and temperature calculations.

$$t_{2,lastSample} = \frac{\tau_{2,lastSample} + t_{prop,2,1}}{\delta_2} \tag{4.7}$$

The calculated clock speed error is also used to determine the true sample period of the

higher designated node.

$$T_{2,s,actual} = \frac{T_{2,s,programmed}}{\delta_2} \tag{4.8}$$

These transformations are then applied to the signal received from the higher designated node. The sample time transformation is applied by calculating the new sample points based on 4.8 and interpolating the raw data. For example, consider this numerical demonstration from a field sample:

$$\tau_{2,lastSample} = 502361\mu s$$

$$T_{2,s,programmed} = 13\mu s$$

$$\delta_2 = 0.9997$$

$$t_{2,lastSample} = 502361\mu s$$

$$T_{2,s,actual} = 13.004\mu s$$

The data points in the node 2 time-series are then plotted along a line with a period of 13.004 μs and a final point at 502361 μs. This effectively aligns the two signals to the same time scale. The effect of this transformation is shown in Fig.4.4.

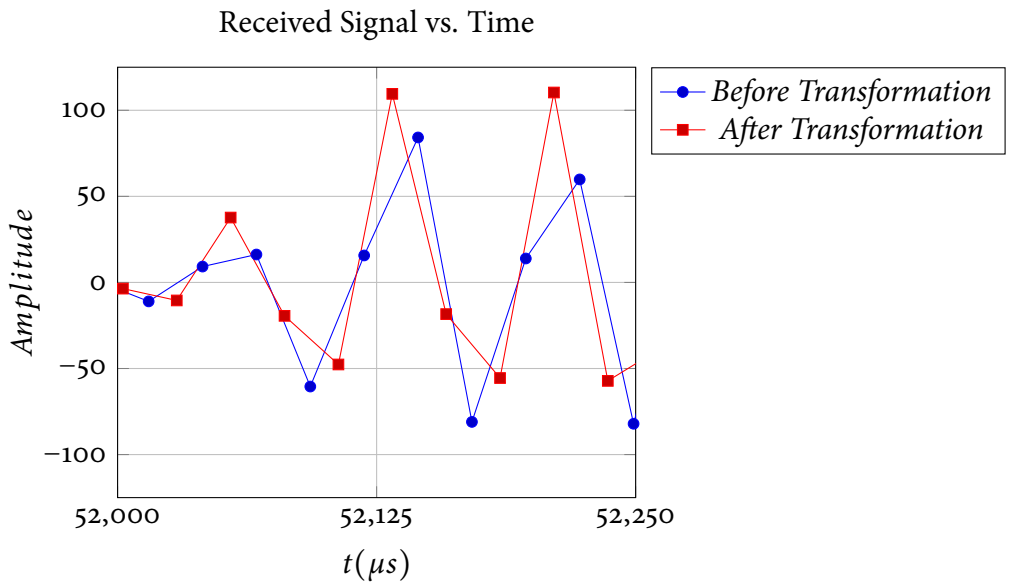

Figure 4.4: Time Shift and Scaling of a Received Signal

As observed in the figure, the shape and position of the waveform is changed by this transformation. It may be more desirable to use more accurate clocks for this purpose but temperatures, moisture, and long periods of extended use in the offshore environment will eventually cause clock drift between controllers in distant locations. This method dynamically corrects for these errors and adapts along with the environment. In practice, this transformation drastically improved the consistency of travel time calculations over collections of samples.

4.3 Travel Time Calculation

Once the time series of the received and transmitted signals have been recorded and aligned to a common clock, the travel time of the wave can be measured. This measurement is completed using matched filtering, also known as autocorrelation. The transmitted wave is shifted, one sample at a time, and multiplied by the received signal. The point where the

signals align will create a peak in their product. The travel time will then result from the number of shifts to reach the peak multiplied by the sample period.

The biggest challenge with using this method in underwater acoustic transmissions is the multipath effect. A single transmitted wave can appear as many overlapping waves at the receiver and the secondary paths often create higher peaks in the cross correlation than the initial wave. Fig. 4.5 shows an incorrect travel time due to multipath error. In the hydrophone 2 to 1 transmission (right-side) the peak in the autocorrelation aligns the signals one period late.

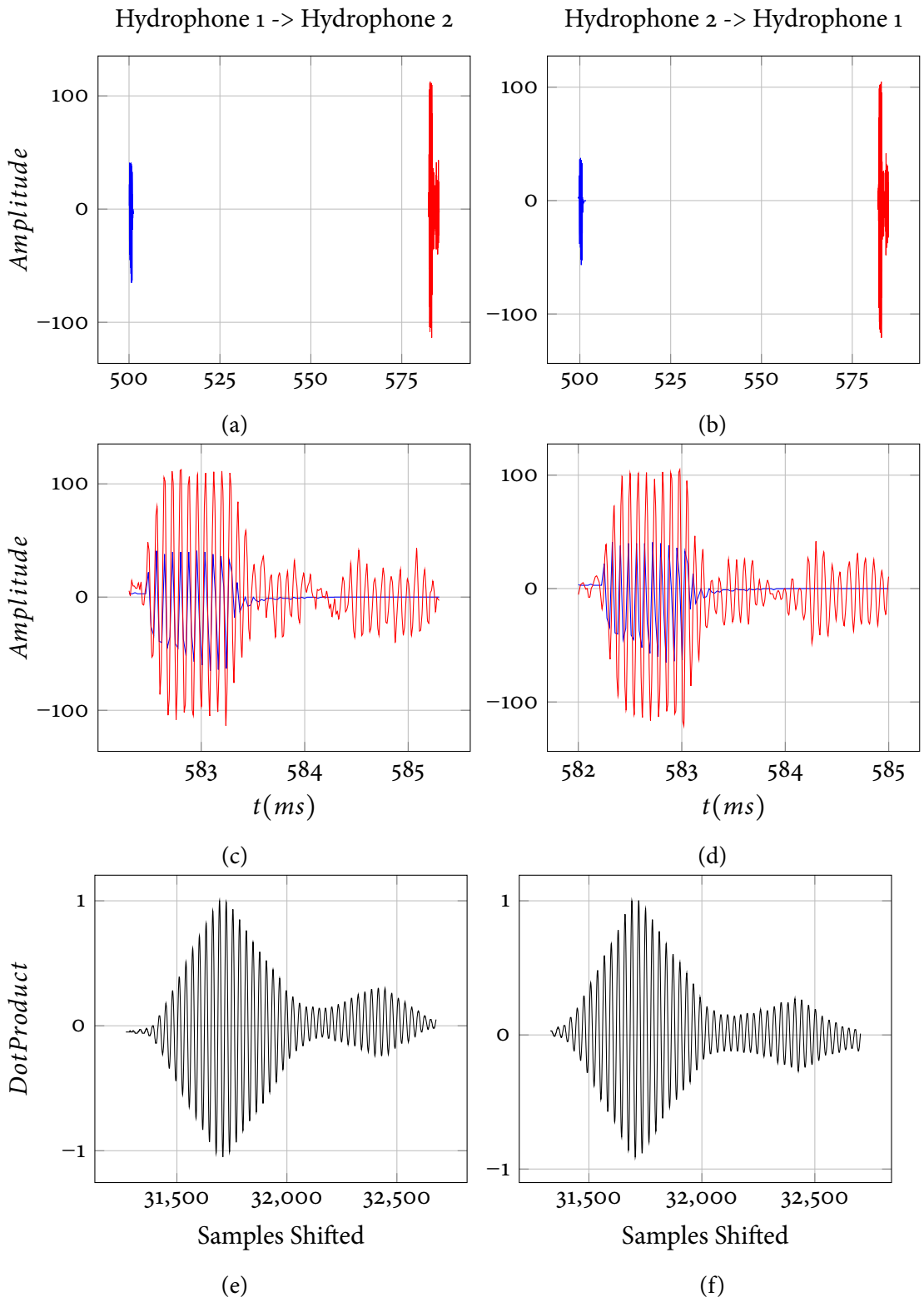

Figure 4.5: Autocorrelation with Multipath Error
Blue: Transmitted, Red: Received
a,b: Full Time Scale
c,d: Zoom-in At Time of Receipt with Shifted Transmission Superimposed
e,f: Auto-correlation Results as T is Shifted Over R

Ideally, a very short pulse would be sent from the transmitter enabling the first arrival to be easily detected. However, a single pulse does not have sufficient energy to be accurately detected at the receiver. Ambient noise and anomalies in the travel path prevent short transmission travel times from being accurately measured. For this reason, longer transmission sequences are desirable but are more prone to misidentified peaks in the cross correlation due to overlapping multipaths.

Binary Phase Shift Keyed transmission sequences are used to help overcome this problem. Longer series of pulses, broken into bits separated by 180-degree phase shifts, create steep peaks in the cross correlation allowing the different travel paths to be easily identified. The following figure shows a transmitted signal with sequence '101' and the corresponding cross correlation output.

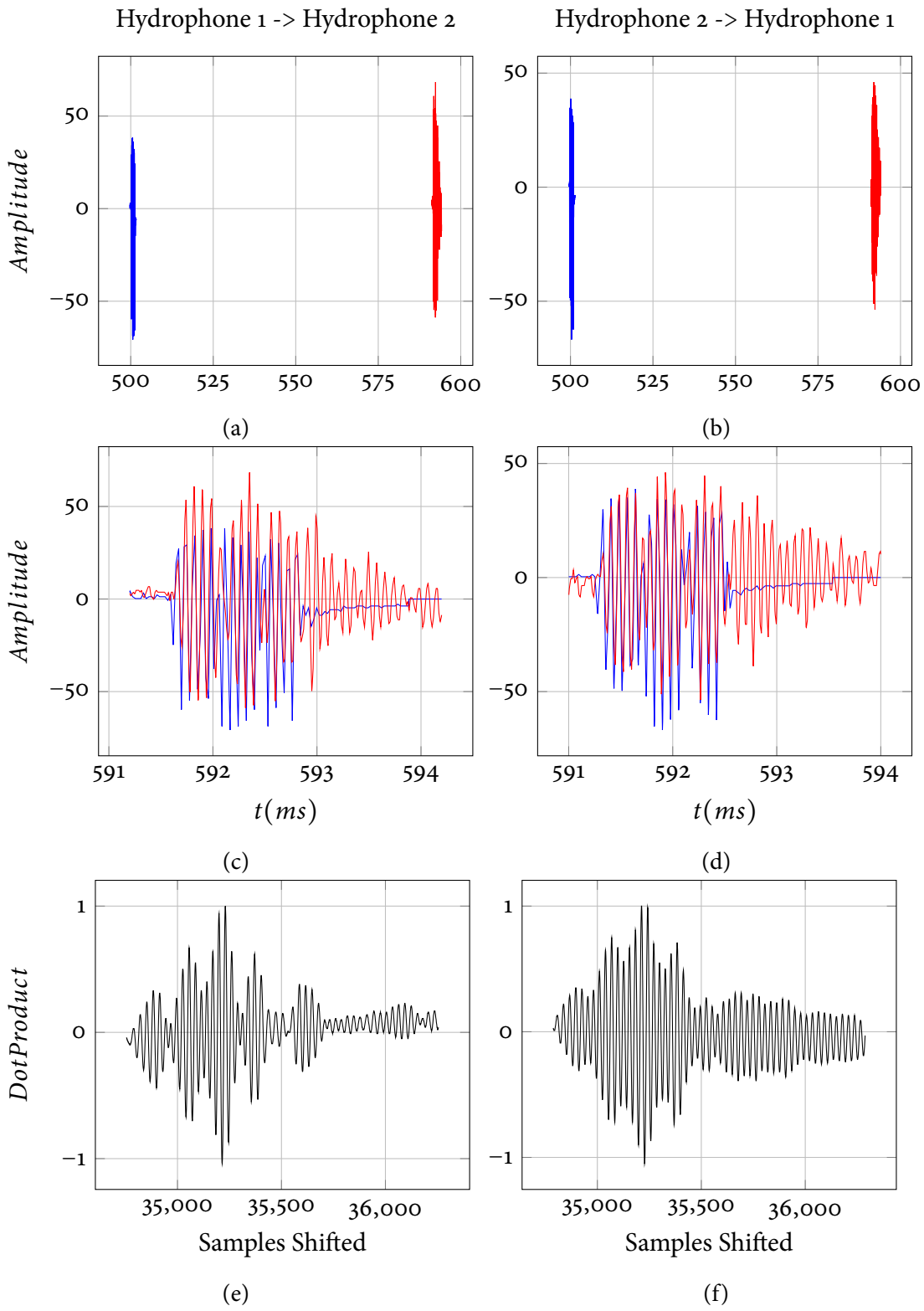

Figure 4.6: BPSK Sequence Autocorrelation
Blue: Transmitted, Red: Received
a,b: Full Time Scale
c,d: Zoom-in At Time of Receipt with Shifted Transmission Superimposed
e,f: Auto-correlation Results as T is Shifted Over R

Comparing the autocorrelation outputs in Fig. 4.6 with Fig. 4.5 shows the benefit of using such a sequence. The steeper peaks and troughs make it easier to resolve overlapping multipaths. This scheme is normally used with much longer sequences, however, this system was limited by the low storage capacity at the receiving node. In practice, even this short sequence provided much more consistency across samples during testing.

Due to the multipath effect, the strongest peak may not correspond with the first arrival time. As such, the processing algorithm records the top ten peaks. The ten peaks in the context of a long series of reciprocal travel times can be used to make informed decisions about which peak to select. More detail is provided on how these peaks are used in the following section.

4.4 Current and Temperature Measurement

This section defines the formulas used to calculate current and sound speed values from the travel time data. The goal is to define the relationship between the acoustic travel times, the temperature, and water velocity along the acoustic path. Each of these derivations begin with the principles outlined in Section 2.1.

The temperature measurement starts with measuring the sound speed based on the sum of differential travel times:

$$\begin{aligned} c &= \frac{v_{1,2} + v_{2,1}}{2} \\ &= \frac{d}{2t_{1,2}} + \frac{d}{2t_{2,1}} \\ &= \frac{d\Sigma t}{2t_1 t_2} \end{aligned} \tag{4.9}$$

The relationship between the speed of sound and temperature used in this work is outlined in [13] and repeated in 4.10:

$$\begin{aligned} c =& 2.1 \times 10^{-4} T^3 \\ &+ \left(-5.44 \times 10^{-2} + 8.7 \times 10^{-5} S + 3 \times 10^{-7} Z\right) T^2 \\ &+ \left(5 - 1.23 \times 10^{-2} S - 9.5 \times 10^{-13} Z^3\right) T \\ &+ 1402.5 + 1.33 S + 1.56 \times 10^{-2} Z + 2.55 \times 10^{-7} Z^2 \\ &- 7.3 \times 10^{-12} Z^3 + 1.2 \times 10^{-6} Z(\Phi - 45) + 1.43 \times 10^{-5} S Z \end{aligned} \tag{4.10}$$

The velocity measurement falls naturally out of the equations defined in Section 2.1, it is derived as follows:

$$\begin{aligned} v_{water} &= \frac{v_{1,2} - v_{2,1}}{2} \\ &= \frac{d}{2t_{1,2}} - \frac{d}{2t_{2,1}} \\ &= \frac{d\Delta t}{2t_1 t_2} \end{aligned} \tag{4.11}$$

These formulas provide averaged temperature and velocity values along the acoustic path. In this work it is assumed that the acoustic path of the earliest arriving wave accurately samples the entire water column between the two nodes. Formula 4.10 can be solved for T by solving the cubic and extracting the real root for a fixed c, S, Z, and Φ. The leading linear terms for T (5) and S (1.33) provide rough guidance on the effect they have on the speed of sound. Both terms are significant and in a deployed system this data could be provided by CTD to improve the absolute accuracy of the measurements.

The first step after a system deployment is to determine the distance between the nodes. This is done by independently measuring temperature and salinity, and calculating the sound speed at the time of deployment with formula 4.9. A transmission sequence is then initiated and the first arrival peak is manually identified by viewing the plot. The distance between the nodes is then calculated using the average travel time:

$$d = \frac{c\Sigma t}{2} \tag{4.12}$$

Once the initial calculation is complete, the distance for this deployment will not change. This enables determination of temperature through the use of formula 4.10. The autocorrelation performed for each transmission pair stores the top n peaks in each direction. This means that the algorithm to determine water temperature and velocity is provided with a set of n possibilities for each of t_1 and t_2. This creates n^2 possibilities for Σt and Δt.

Identification of the correct peak uses the fact that water velocity between two points will not increase rapidly from one sample to the next. An error in peak identification will cause a jump of at least one period of the acoustic frequency (in this case 80 μs) in the measured travel time from one sample to the next. An 80 μs jump in travel time corresponds to a 60 cm/s change in current speed at 150m distance. At a sample interval of approximately two minutes, this size of a jump is extremely unlikely.

First, the algorithm is seeded with an initial expected velocity by manually analysing the first transmission set. The $[t_1, t_2]$ for the second transmission is selected as the pair that provides the closest Δt to the manually analysed reading. Once z transmission pairs have been analysed in this way a running, weighted average is used for the expected Δt. The expected Δt is a weighted average of the previous z samples. This allows peaks that would create sudden jumps in water velocity to be rejected. Utilizing neighbourhood information and informed knowledge about a measurement parameter is a common technique. An early

paper describing one such method is [23].

This method is more effective for calculating velocity than temperature. It exploits the fact that the wave will travel the same path in both directions - meaning that the multipaths will be the same for both t_1 and t_2. The algorithm will not always choose the first wave arrival but will always choose matching ray arrivals for t_1 and t_2. This methodology enables determination of differential travel times, however it results in some high frequency noise in temperature data that can be observed in the dataset.

4.5 Error Analysis

The errors in the travel time measurements are a factor of the errors in hardware and physical factors of the wave motion. The physical anomalies such as cross currents, and momentary shifts are not considered in this work and the following assumptions are used:

- The waves travel directly from the transmitter to the receiver.
- Any changes in the ocean between the upstream and downstream transmissions are negligible.

The error analysis in the velocity and temperature calculations both begin with the distance determination. The distance is a fixed factor and is determined upon launch based on the following formula:

$$d = \frac{c\Sigma t}{2} \tag{4.13}$$

e_d (error in distance measurement) can be determined by considering the errors e_c and e_t. e_c is proportional to the error in an initial, independent, temperature measurement. A 1

degree error in this temperature measurement translates to an e_c of 4 m/s.

This work assumes that the salinity, depth, and latitude are constant. Some of these factors, particularly salinity, have a significant impact on the absolute error and would need to be independently measured with a CTD instrument in a real application. For this proof-of-concept testing, constant approximations are used, as a CTD instrument was not available.

The hardware and software induced delays are of the most interest in this work, as these cannot be removed with complimentary data measurements from a CTD. We can negate clock drift between the controllers here, as that is measured and removed from the calculations as described in Section 4.3.

To determine the delays introduced by the hardware and hydrophones we define the following terms:

- $t_{t,actual}$: True time the acoustic pulse leaves the transducer.
- $t_{t,reported}$: Time of acoustic pulse recorded at transmitter.
- $t_{t,filters}$: Time for the signal to pass through the transmitter signal processing hardware.
- $t_{r,actual}$: True time the acoustic pulse arrives at receiver.
- $t_{r,reported}$: Time of acoustic pulse recorded by receiver.
- $t_{r,filters}$: Time for the signal to pass through the receiver signal processing hardware.
- t_{hydro}: Delay between the motion of the hydrophone and a signal appearing at the input to the signal processing hardware.

The actual time of transmission will be slightly later than reported as the wave is recorded

electrically. In practice there will be a delay between a voltage being applied to the hydrophone terminals and the mechanical reaction. The delays induced by the filters and ADC must also be subtracted.

$$t_{t,actual} = t_{t,reported} + t_{hydro} - t_{t,filters} \tag{4.14}$$

The actual time of receipt will be slightly earlier than reported as the mechanical/electrical lag in the piezoelectric sensor is included in the reported time. The receiver circuit also has it own signal processing and ADC which will induce delays.

$$t_{r,actual} = t_{r,reported} - t_{hydro} - t_{r,filters} \tag{4.15}$$

The true travel time is:

$$\begin{aligned} t_{actual} &= t_{t,actual} - t_{r,actual} \\ &= \left(t_{r,reported} - t_{hydro} - t_{r,filters}\right) - \left(t_{t,reported} + t_{hydro} - t_{t,filters}\right) \\ &= \left(t_{r,reported} - t_{t,reported}\right) - 2t_{hydro} - t_{r,filters} + t_{t,filters} \end{aligned} \tag{4.16}$$

And so it follows that:

$$e_t = -2t_{hydro} - t_{r,filters} + t_{t,filters} \tag{4.17}$$

The filter induced delays were measured in the lab. These were determined to be on the order of ns and can be neglected. That leaves the delay from the piezoelectric hydrophones, which can go as high as one period of the sinusoidal input signal. Adding these error terms

to the distance calculation results in the following:

$$e_d = \frac{(c + e_c)(t_1 + t_2 + 2e_t)}{2} - \frac{c(t_1 + t_2))}{2} \tag{4.18}$$

After the initial calculation of distance, the travel times are used to determine sound speed. The following formula is used:

$$c = \frac{d\Sigma t}{2t_1 t_2} \tag{4.19}$$

Adding the error terms to the d and t terms gives the following error for c:

$$e_c = \frac{(d + e_d)(\Sigma t + 2e_t)}{2(t_1 + e_t)(t_2 + e_t)} - \frac{d\Sigma t}{2t_1 t_2} \tag{4.20}$$

The water velocity is determined from the following equation:

$$v = \frac{d\Delta t}{2t_1 t_2} \tag{4.21}$$

Adding the error terms gives the following:

$$e_v = \frac{(d + e_d)(\Delta t + e_{\Delta t})}{2(t_1 + e_t)(t_2 + e_t)} - \frac{d\Delta t}{2t_1 t_2} \tag{4.22}$$

Note the introduction of the $e_{\Delta t}$ term to the error numerator. Ideally the errors in t_1 and t_2 would cancel perfectly and the Δt term would be exact. In practice however, small differences in the travel time calculations in each direction create a small error in Δt. The value of $e_{\Delta t}$ is difficult to quantify and so was determined experimentally to be approximately $\pm 5us$. The details around this determination are discussed further in Section 5.1.

The different errors present themselves in the data in different ways. As the distance calculation is performed once, the error in distance creates a constant offset across all data. The errors in travel times also have a constant bias term resulting from the hydrophone delay. This delay may fluctuate with temperature but changes relatively slowly. The error in Δt and small errors in the travel time calculation vary rapidly and appear as high frequency noise in the data.

4.6 User Interface

The experimental nature of the work required the ability to change system operating parameters during testing. A simple command-line based user interface was developed which enables the user to send commands to the underwater nodes from onshore. Commands are entered at the data collection PC connected to the master node via USB and relayed to the underwater nodes. The syntax of a command is as follows:

$$NodeNumber, Command, Parameter$$

The following is a list of valid commands to the system and a brief description of their effect.

Command	Parameter	Description
br	Baud Rate	Changes the Modbus Baud Rate (triggers a system reset).
ct	Communications Timeout	The time in milliseconds for a node to wait for a Modbus message from the master before resetting itself.
da	Date	The current date. used to track time for naming of data files on the SD card.
dp	Data Points	Changes the number of Data Points saved during a transmission.

Command	Parameter	Description
dt	Delay Time	The time in milliseconds for a node to wait after receiving its role before initiating its receive or transmit.
ft	First Transmitter	Sets which node transmits first upon startup.
ga	Gain	Manual entry of hydrophone receiver gain.
gl	Gain Level	Sets the hydrophone input amplifiers at the nodes to a preset pair of gain values.
hi	High Speed Modbus	Sets the baud rate to 9600bps and the polling rate to 50ms (triggers a system reset).
in	Initialize	Sets the values stored in the EEPROM of the nodes and master to a set of default values.
lo	Low Speed Modbus	Sets the baud rate to 2400bps and polling rate to 200ms (triggers a system reset).
mi	Minute	The current minute. used to track time for naming of data files on the SD card.
mu	Mute Toggle	The system will operate without sending signals to the hydrophones.
nc	Number of Cycles	The number of complete cycles of the transmission sequence to repeat.
np	Number of Pulses	The number of pulses in a single bit of the transmission sequence.
ns	Number of Synchs	Sets the number of synchronization pulses sent to the nodes during each transmission cycle.
pr	Polling Rate	The Modbus polling rate in ms.

Command	Parameter	Description
re	Reset	Sends a reset command to the nodes and then resets the master.
sd	SD Toggle	Enables and disables writing to the SD card.
se	Sequence	An integer representing the BPSK sequence pattern transmitted by the nodes.
tt	Timer Top	Changes the frequency of the hydrophone transmissions.

Table 4.1: User Interface Commands

These commands were most useful during setup and initial testing. The commands made it possible to experiment with different acoustic transmission sequences to determine the optimal pattern in a new environment. As each transmission is read back and stored by the transmitter, the matched filtering adapts along with changes in the sequence.

As an example, consider the following sequence of commands:

- 3, se, 27
- 3, tt, 127
- 3, np, 5
- 3, se, 2

This sets the BPSK transmission sequence to '11011' (27), the timer top to 127 (corresponding to a transmission frequency of 12.5 kHz), the number of pulses per bit to 5, and the number of sequences to 2. The acoustic transmissions will then be set to a stream of 50 pulses at 12.5kHz in the pattern '1101111011' where each binary number consists of 5 periods and a

transition between '0' and '1' corresponds to a 180-degree phase shift. These parameters can be easily modified 'on-the-fly' to adapt to different deployment environments.

To achieve high resolution in the measured travel times, sequences which create the sharpest peaks when autocorrelated are desired. In practice, pseudorandom m-sequences are used to achieve this as outlined in [22]. A pseudorandom m-sequence is a periodic sequence which generates every possible representation of the bits in the sequence (except all zeroes). These sequences provide the highest SNR gain when autocorrelated. The space limitations at the receiving controller prevented this system from using the full benefit of these sequences. However, the software is designed to support any length of such a sequence and to allow for field changes. These values could be modified after deployment to determine the best sequence for a given deployment environment.

Chapter 5

System Testing

The system has been tested extensively both in the lab, and in the field. The first tests were performed on the laboratory bench with the hydrophones transmitting through the air. Hydrophones are not optimized for use out of water and so only limited testing was possible this way. Further testing and verification was done in the deep tank at the Memorial University hydraulics lab. The highly reflective environment of the tank created problems with signal detection. Large bodies of open water were required for the full system tests.

The first field tests were done under ice cover in Long Pond near Memorial University in St. John's. There was very little current in Long Pond during the winter season, but findings were close enough to readings from an ADCP to warrant testing in more difficult environments. The system was deployed in Bellevue, NL for a two day period during summer 2019 to measure tidal currents. This trial yielded successful results and provided valuable insight into the possibilities of the system.

5.1 Lab Verification of Travel Time Accuracy

Travel times of acoustic waves through the air were used during design and development. The hydrophones can detect signals from short distances when out of water. This, combined with the property that the differential travel time between two waves travelling through still air should be zero, was utilized to refine and test the system in the lab. Fig. 5.1 shows the result of a differential transmission through the air in the lab at a separation distance of approximately 1.3m.

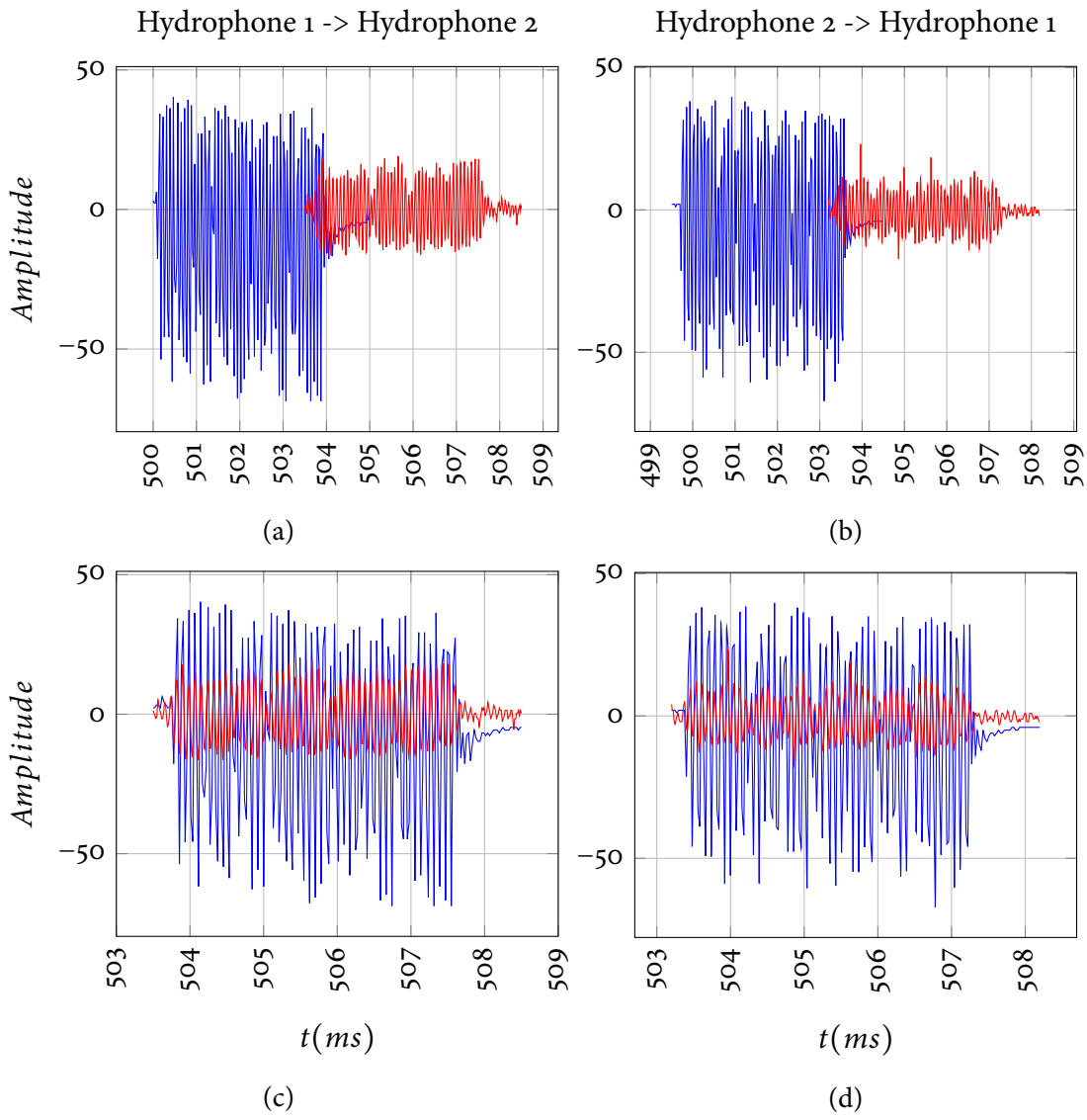

Figure 5.1: Travel Time Testing in Lab
Blue: Transmitted, Red: Received
a,b: Full Time Scale
c,d: Zoom-in At Time of Receipt with Shifted Transmission Superimposed

The travel time in both directions in this transmission was measured to be 3676.4 μs. At an expected speed of sound through air of 343 m/s, this should correspond to a measured distance of 1.26m. A metre stick was used to measure the distance of the hydrophones at 1.2m. As the measured distance was between the edge of the rubber covers of the hydrophones, the

cover thickness likely contributed to the error.

The system was designed to specification such that the differential travel time between the two nodes at this distance would not exceed 5us. To ensure this functionality, the system was left to run for a 2 hour span, sampling every two minutes. The Δt for each transmission pair was then verified to ensure conformance to specification. This testing allows $\pm 5\mu s$ to be used as the error in Δt for the error analysis.

This method was also used to determine the sensitivity of the system. Moving the two hydrophones closer should produce shorter travel times. With an assumed sound speed of 343 m/s, a 1 mm movement in a hydrophone should produce a travel time change of $2.9\mu s$. Fig. 5.2 shows a picture of the distance testing setup in the lab.

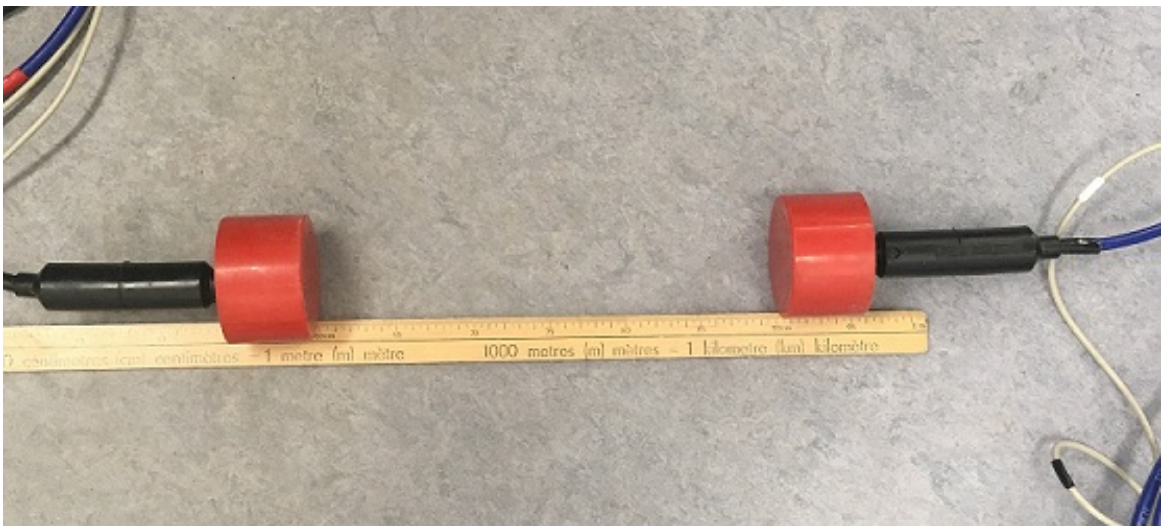

Figure 5.2: Lab Testing of Distance Sensitivity

This setup was used to capture 45 samples at a distance of approximately 1.26m. After 45 samples the distance was increased by 1mm and another 45 samples were captured. The plot of the data from this testing is shown in Fig. 5.3. From the data it can be seen that the system could reliably detect 1mm changes in position if averaging over at least five readings. This result led to the design of the system to continuously send transmissions to maximize

the amount of data retrieved for a deployment.

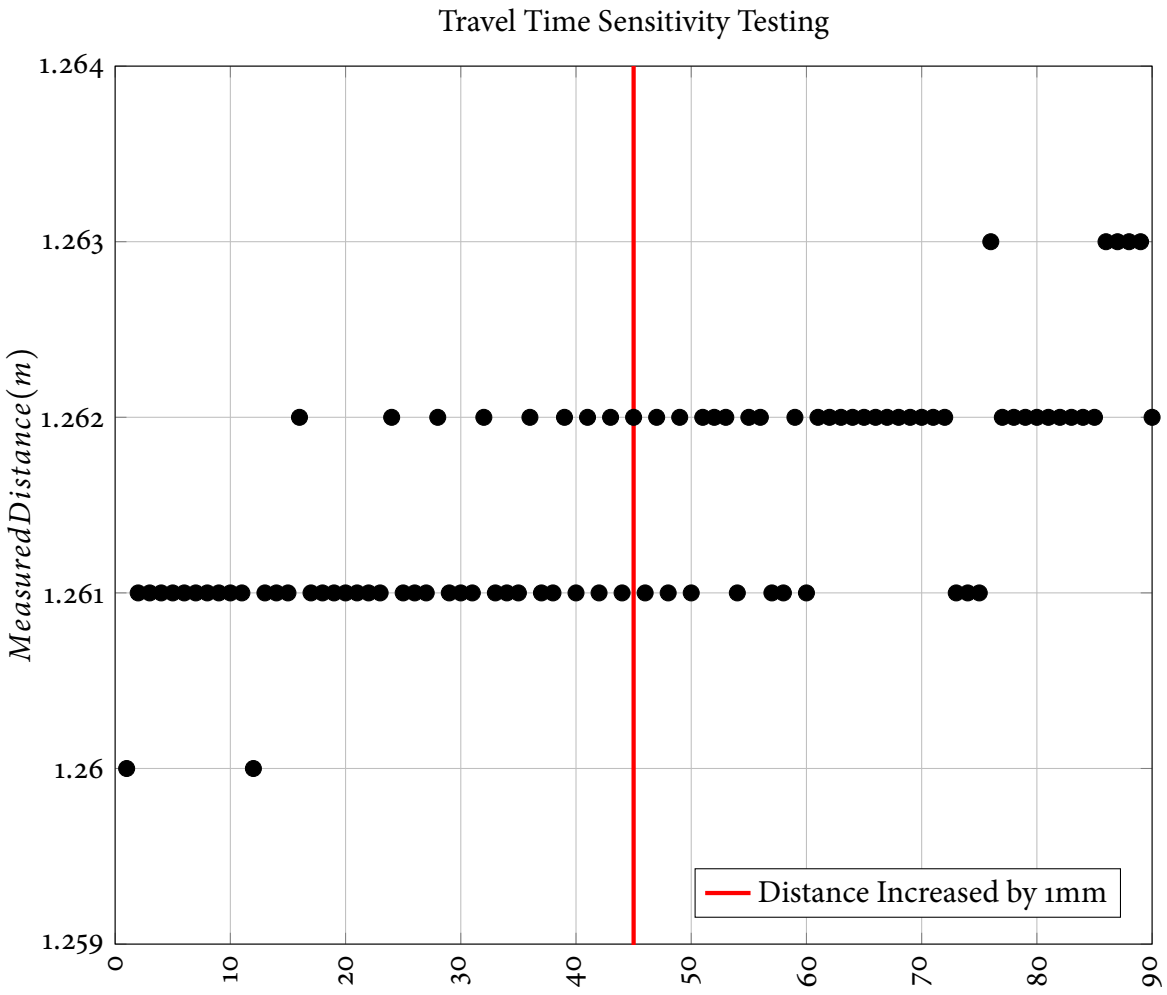

Figure 5.3: Distance Based Sensitivity Testing in Lab

These tests also acted as a calibration of the entire system as all components were utilized. The absolute accuracy of a single travel time measurement was difficult to determine as the thickness of the hydrophone covers was not known.

5.2 Long Pond Winter 2019: Measurements Under Ice

The first field tests of the system were performed in Long Pond during the winter of 2019. The ice cover simplified the launching process as the hydrophones were suspended through holes in the ice and the electronics enclosures stayed dry atop the ice. Fig. 5.4 shows a top down view of the node positioning. The data presented here is from the 120m separation point. Fig. 5.5 shows a ground level view from the location of node 1.

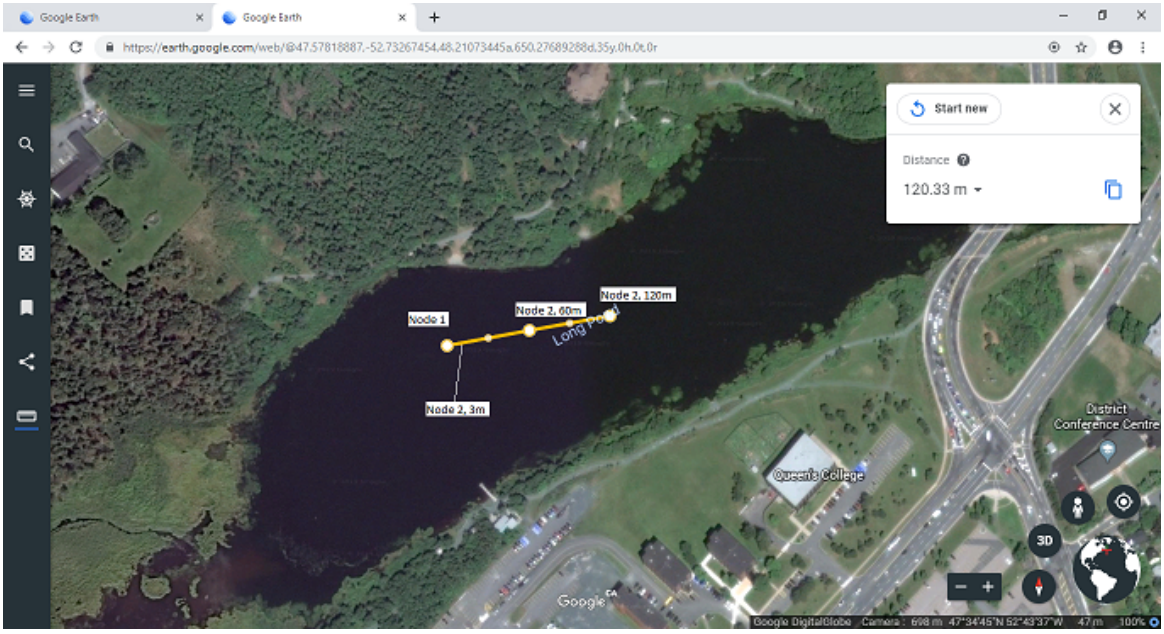

Figure 5.4: Long Pond Testing February 2019 Top-Down View

Figure 5.5: Long Pond Testing February 2019 Ground Level View

In this test the hydrophones were suspended through the ice at a separation distance of 120m. Travel times were measured at a number of different depths by lowering the hydrophones in controlled steps. An ADCP was also deployed for comparison to the system measurements. Fig. 5.6 shows the data comparison of the two measurement methods.

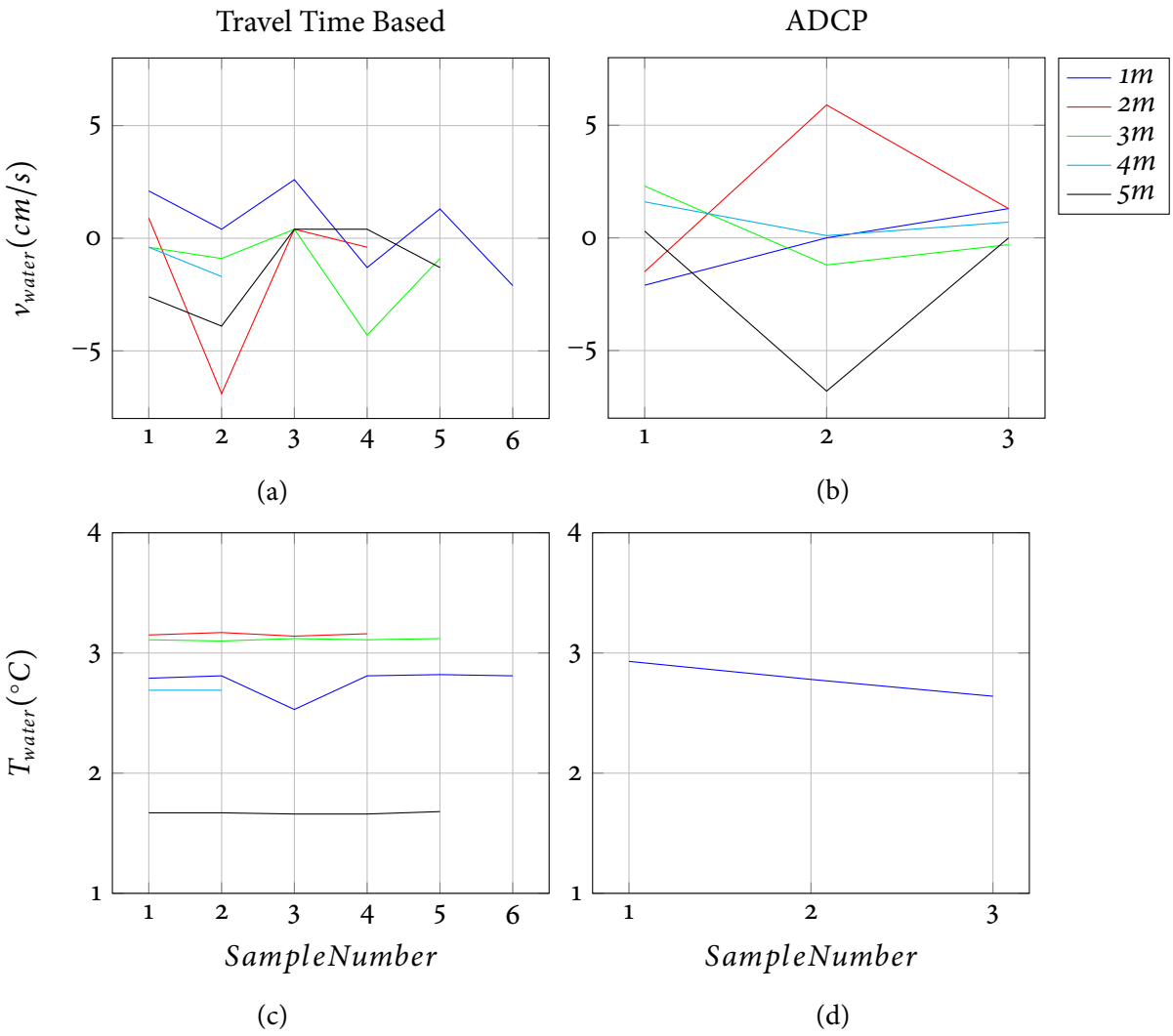

Figure 5.6: ADCP and Travel Time Based Data Comparison
a: Travel Time Based Velocity, b: ADCP Velocity (East Component)
c: Travel Time Based Temperature, d: ADCP Temperature Sensor

A notable result from this testing was the clarity of the data at the shallowest depths. It is suspected that this was due to the hydrophones being close to the reflective ice layer. The angle of reflections from the ice were thus shallower and interacted less with reflections from the bottom and axial travel paths. Fig. 5.7 shows a comparison of the quality of the received signal at depths of 1m and 4m.

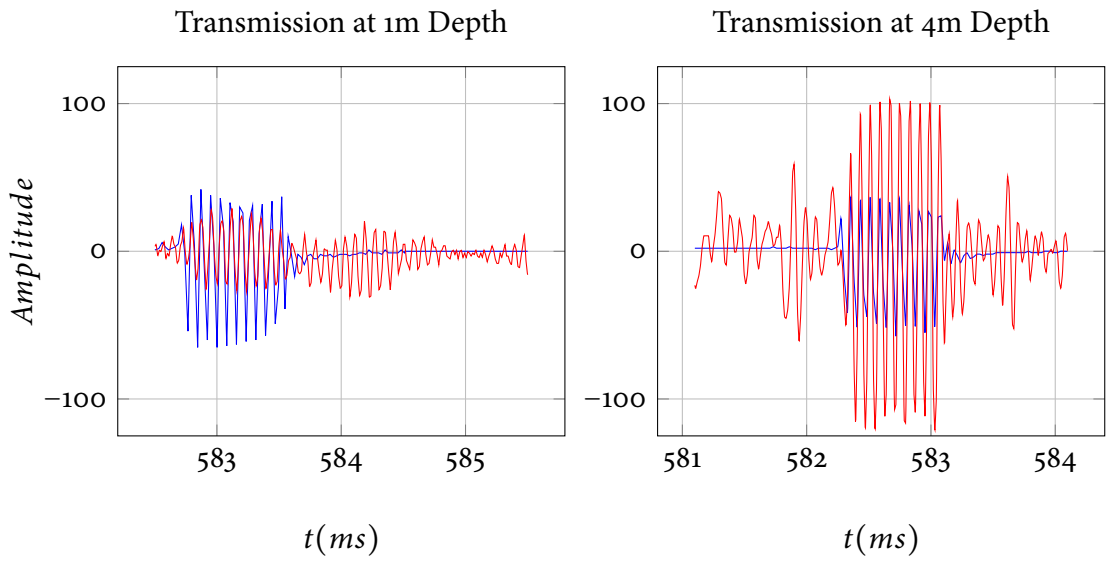

(a) (b)

Figure 5.7: Long Pond Depth Comparison
Blue: Transmitted, Red: Received
a: Easily Separable Paths at 1m Depth
b: Destructive Multipath Interference at 4m Depth

In this testing, a SonTek Argonaut XR was used to measure the temperature of the water. The average temperature reading was $2.8°C$ and SonTek claims an accuracy of $\pm 0.1°C$ in the product datasheet. Working through the error formulae as outlined in Section 4.5 gives the following error values:

- $e_d = 0.27m$
- $e_T = 1.57°C$
- $e_v = 4.3cm/s$

The water in Long Pond was not moving fast enough to surpass the expected error value. While the results were promising, and in alignment with the ADCP data, faster moving water was needed to verify the system.

5.3 Bellevue Summer 2019: Tidal Current Measurement

Bellevue is a town on the Northeast coast of Newfoundland. It has a natural channel near the coast where water is concentrated to funnel in and out of during tide changes. This creates predictably varying currents, making the area ideal for testing the current measurement system. Fig. 5.8 shows a topographic view of the test setup.

Figure 5.8: Bellevue Testing August 2019 Top-Down View

The subsea nodes and hydrophones were attached to steel frames and deployed from kayaks. Fig. 5.9 shows the system deployment setup. Node 2 came to rest in about 4m of water and the hydrophone was fastened about 1m from the bottom. Node 1 was placed in approximately 1.5m of water at low tide and its hydrophone was also fastened 1m from the bottom.

Figure 5.9: Bellevue Testing August 2019 Ground Level View

Once it was confirmed that the signals were being captured and the node gains were balanced, the system was left to run autonomously for approximately 48 hours. This was long enough to capture 4 complete tide cycles. A fishing vessel caught the buoy from node 2 in its propeller on day 2 of the deployment. This resulted in the frame being tipped and the hydrophone coming to rest in silt. There is significant degradation in the quality of the signals from Node 2 after this point, which is observed in the data.

Fig. 5.10 shows the time-series of the current and temperature measurement of the system during this testing. Positive velocity in this case is defined as water moving away from Node 1 (tide coming in) and negative velocity is water moving towards Node 1 (tide going out).

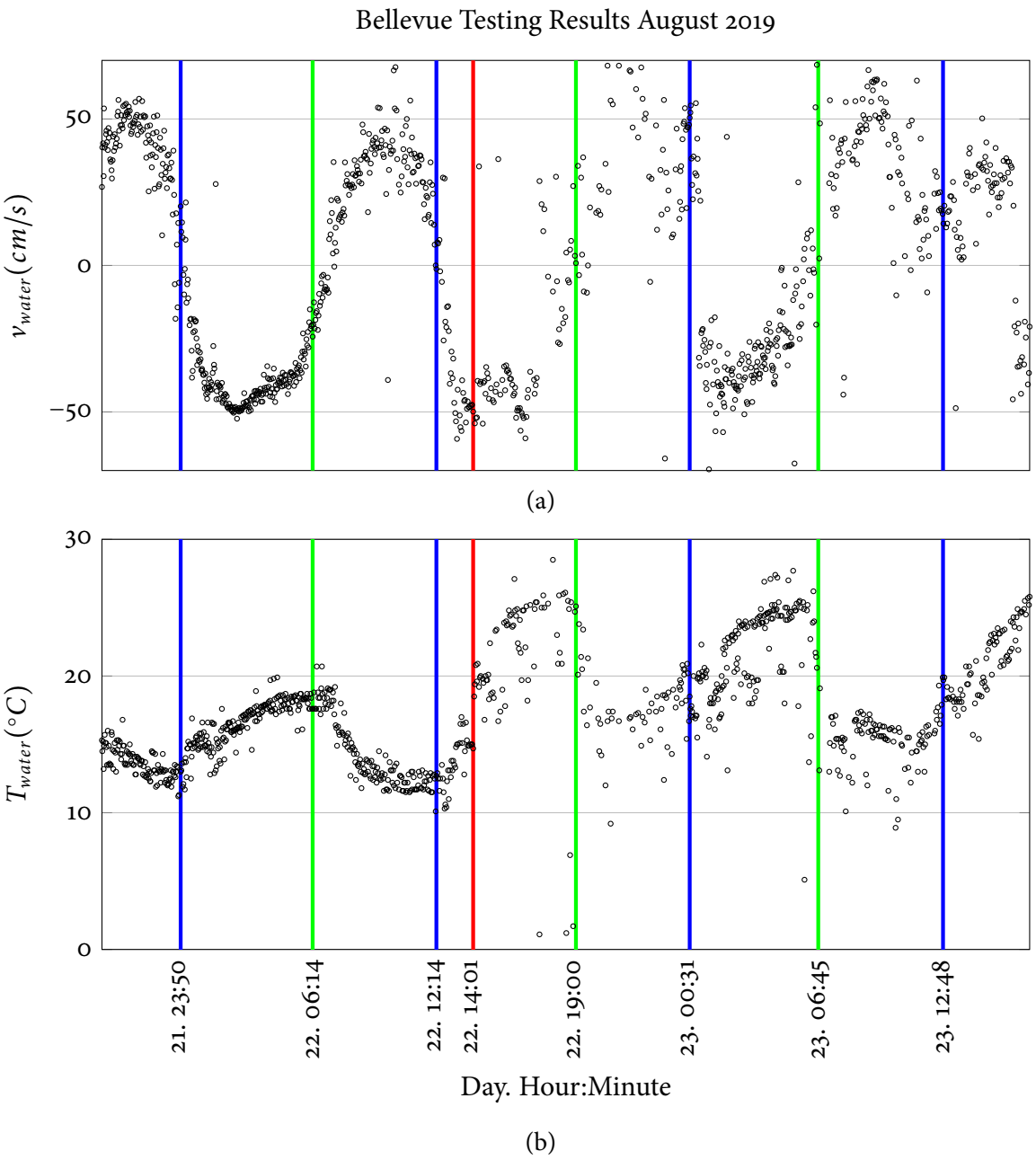

Figure 5.10: Current and Temperature from Bellevue Testing August 2019
Tide Predictions from https://www.waterlevels.gc.ca/
Blue: High Tide, Green: Low Tide, Red: Propeller Strike
a: Water Velocity (+v: Tide Coming, -v: Tide Going Out)
b: Water Temperature

There are several observations that can be made from this data. The zero-crossings align

closely with the predicted high and low tides as expected, as this is where the current changed direction. The velocity and temperature curves are approximately 180 degrees out of phase. This is because when the tide was going out (positive flow), the water flowing past the hydrophones was coming from the shallow bay in Bellevue and the water had been warmed by the sun. When the tide was coming in, colder ocean water was flowing past the hydrophones.

The assumption of constant salinity (35 parts per thousand) caused some error in the temperature data. While the tide was going out, the water was fresher as it included run-off from streams in the area. This limits the absolute accuracy of the testing data. However, the relative values and trending when compared to expected high and low tide levels still provide proof-of-concept of this method. In a commercial or scientific deployment of such a system, better absolute accuracy could be attained by using complimentary data from a CTD.

Looking at the section of data before the propeller strike shows that the zero crossings align closely with the predicted high and low tides from [20]. After the propeller strike the data becomes much more scattered due to the degradation of the signals from the hydrophones. Even in this range, most of the data is in the positive range after low tide and the negative range after high tide. The shift in temperature data was caused by a change in distance between the nodes after the propeller strike. Fig. 5.11 shows the effect of this event on the quality of the acoustic data.

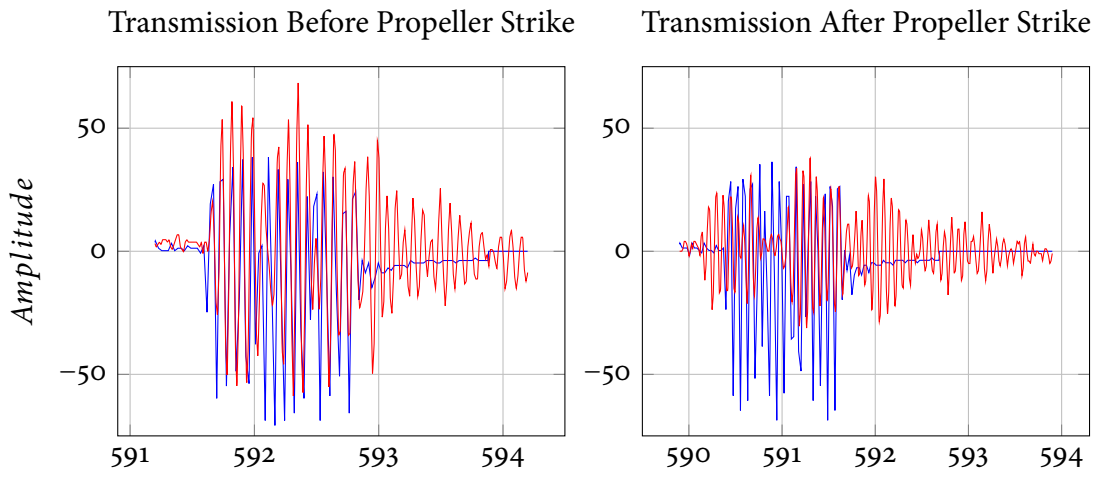

(a) (b)

Figure 5.11: Propeller Strike Effect on Data Quality
Blue: Transmitted, Red: Received
a: High Quality Transmission Before Propeller Strike
b: Low Energy Transmission After Propeller Strike

A water temperature estimate of $14.8°C$ was used for the initial node distance calculation. As no temperature monitoring instrument was available, and absolute accuracy was not the goal of this demonstration, a temperature error estimate of $\pm 1°C$ is used for the error analysis. As was the case with the salinity, these measurements could be improved with independent instruments which are readily available in practice but were not available for this testing. Working through the error formulae outlined in Section 4.5 yields the following error values:

- $e_d = 0.55m$
- $e_T = 2.25°C$
- $e_v = 4.0cm/s$

Note that errors for distance and temperature are higher than for the Long Pond testing, while the error in water velocity is lower. This is because the Bellevue testing has a higher

initial temperature uncertainty but a greater distance between the nodes. These error values only apply to the period of data before the propeller strike. After the propeller strike the quality of received data was degraded to a point that the ability of the system to measure travel times accurately was hindered. This can be seen clearly by the increase in scattered points after the strike.

Chapter 6

Conclusions

This was a challenging project which stretched across many disciplines. The nature of the parameters being measured made modelling and testing extremely challenging. Despite these things it was still possible to produce favourable results with limited equipment. The data from the Bellevue deployment demonstrates that the method is sound, and it is possible to measure currents at short ranges using reciprocal travel times.

Further development of these ideas using more capable hardware could produce better results. Input from oceanographers and physicists could yield more effective acoustic signal patterns. The novel concept of recording each transmission before applying matched filtering makes it possible to trial different signal patterns without reprogramming the controllers.

The value of this technology is the resultant single-axis current meter, which does not suffer from the erratic measurements of single-point detectors. The technology could be easily extended using the concepts noted above to develop a more powerful tomography network capable of measuring new acoustic paths and producing high resolution, real-time, current maps.

6.1 Lessons Learned

The goal of this project was to determine the feasibility of using differential travel time to measure ocean currents at short ranges. The testing phase included several failed attempts and design changes before obtaining the results included in this thesis. Some insight was also gained along the way into opportunities for reducing the system error.

The initial set of field tests in Long Pond included three attempts before final results were collected on the fourth try. These tests revealed the sensitivity of Arduino clock drift to temperature. Given the importance of clock synchronization to the results, it is necessary to have a dynamic measurement of clock drift as it can change drastically with changes in the deployment environment. Later attempts revealed the sensitivity of the communications circuits to changes in temperature and humidity. It is a necessity to test these designs in the expected conditions of the environment.

The ice-covered pond provided a great test environment for the system. It is much easier to walk across the ice with the equipment and deploy through holes in the ice than it is to deploy from a boat. In a design that is impossible to test in a reasonably sized tank due to the reflection of acoustic waves in that environment, a frozen pond or lake provides a suitable test area.

While many of the electrical and software issues were resolved following the Long Pond deployment, some mechanical traps presented themselves during the first test in Bellevue. The frames constructed for the first test were not sufficiently weighted to remain stationary in the strong tidal currents. The system was deployed for approximately one hour before enough kelp built up on the hydrophone cables to catch the current and uproot the hydrophone mounts. The final test used heavier test frames, with cables kept as low and direct as possible to avoid build up of drifting materials.

The propeller strike on the second day of deployment in Bellevue caused a degradation of the data in that period. An identification buoy was clearly marked and close to a pre-existing buoy in the area, so there was little more that could have been done to avoid such an encounter. It is interesting to observe the effect of this event on the ability of the system to measure the current. The values after the strike are more scattered but remain qualitatively similar. The susceptibility of such a system to major environment changes such as this would depend on the required accuracy. While a wireless system with GPS synchronization would be more resilient to environmental events, it would require more expensive and specialized hardware to build and maintain. Any decision on which type of system is required for a specific application would need to consider these factors.

This work can also provide some quantitative analysis for deployment considerations. Accuracy of the current measurement is directly proportional to the distance between the two nodes. The nodes in the Bellevue test were approximately 130m apart which translated to an expected error in the current measurement of 4.0 cm/s. This error comes with the caveat that we are assuming uniform current over the acoustic path, although more nodes could be added to increase resolution if required. This area contained currents on the order of $\pm 50 cm/s$, making the error acceptable for demonstrating the method. In open ocean, however, currents are much lower and rarely exceed 10 cm/s. The distance between the nodes could be increased to achieve the accuracy required in such a deployment. A separation distance of 1 km would provide a much lower error value of 0.8 cm/s.

A major hindrance to accuracy in this system is the power-over-data design. This design allowed testing to proceed at long distances as the only cable that was available was two-core. However, the power-over-data design creates a large amount of noise in the power supply for the hydrophone amplifier circuit. It is anticipated that isolating the data and power would create much cleaner hydrophone signals and would reduce the all-important error in Δt

below $5\mu s$. With an error in Δt of 2 μs and node separation distance of 1 km, the error in velocity would be 0.3 cm/s. Error values in this range may be acceptable in an iceberg monitoring or environmental study application.

6.2 Future Work

There are several options to further develop the work presented in this thesis. An experimental verification of the claim that errors could be greatly reduced by isolating data and power and increasing node separation would be valuable. If these lower errors could be verified the natural progression would be to increase the number of nodes and acoustic paths. A network of four underwater nodes surrounding a $1km^2$ area would provide an invaluable demonstration of these methods. Such a system, however, would require significant investment and deployment planning.

Another possible avenue for development is in data-processing. The data from the Bellevue test provides a sample of both high- and low-fidelity transmissions. An investigation into numerical analysis methods could determine if a cleaner sinusoid could be extracted from the cross-correlation peaks. This work uses a relatively simple running weighted average to choose which peak to interpret as the travel path but a neural network may enable more accurate classifications.

Bibliography

[1] Y. Adityawarman, A. Kaneko, K. Nakano, N. Taniguchi, K. Komai, X. Guo, and N. Gohda. Reciprocal sound transmission measurement of mean current and temperature variations in the central part (aki-nada) of the seto inland sea, japan. *J. Oceanogr.*, 67:173–182, 04 2011.

[2] D. Behringer, T. Birdsall, M. Brown, B. Cornuelle, R. Heinmiller, R. Knox, K. Metzger, W. Munk, J. Spiesberger, and R. e. a. Spindel. A demonstration of ocean acoustic tomography. *Nature*, 299(5879):121–125, 1982.

[3] B. Dushaw, A. Forbes, F. Gaillard, A. Gavrilov, J. Gould, B. Howe, M. Lawrence, J. Lynch, D. Menemenlis, J. Mercer, P. Mikhalevsky, W. Munk, I. Nakano, F. Schott, U. Send, R. Spindel, T. Terre, P. Worcester, and C. Wunsch. Observing the ocean in the 2000's: A strategy for the role of acoustic tomography in ocean climate observation. In *In: Koblinsky, C.J., and N.R. Smith (Eds.): Observing the Oceans in the 21st Century. GODAE Project Office and Bureau of Meteorology*, pages 391–418, 2001.

[4] B. D. Dushaw. Ocean acoustic tomography in the north atlantic. *Journal of Atmospheric and Oceanic Technology*, 36(2):183–202, 2019.

[5] Falmouth Scientific, Inc. *ACM-PLUS 3-Dimensional Acoustic Current Meter User Manual*.

[6] Falmouth Scientific, Inc. *ACM-PLUS Brochure*.

[7] K. Hessner, S. El Naggar, v. Appen, and Strass. On the reliability of surface current measurements by x-band marine radar. *Remote Sensing*, 11:1030, 04 2019.

[8] N. G. Hogg and D. E. Frye. Performance of a new generation of acoustic current meters. *Journal of Physical Oceanography*, 37(2):148–161, 2007.

[9] B. M. Howe, P. F. Worcester, and R. C. Spindel. Ocean acoustic tomography: Mesoscale velocity. *Journal of Geophysical Research*, 92(C4):3785, 1987.

[10] S. Ishii, G. Kai, T. Hara, and I. Nakano. Us patent 4805160: Data transmission method for ocean acoustic tomography, 1989.

[11] K. Kawanisi, A. Kaneko, M. Razaz, T. Abe, C. Zhang, and H. Tang. *Measurement of Cross-Sectional Average Velocity in a Shallow Tidal River with a Next-Generation Acoustic Velocity Meter*, pages 1972–1977. 01 2009.

[12] K. Kawanisi, M. Razaz, J. Yano, and K. Ishikawa. Continuous monitoring of a dam flush in a shallow river using two crossing ultrasonic transmission lines. *Measurement Science and Technology*, 24:055303, 03 2013.

[13] C. C. Leroy, S. P. Robinson, and M. J. Goldsmith. A new equation for the accurate calculation of sound speed in all oceans. *The Journal of the Acoustical Society of America*, 124(5):2774–2782, 2008.

[14] W. Munk, P. Worcester, and C. Wunsch. *Ocean Acoustic Tomography*. Cambridge University Press, 1st edition, 1995.

[15] W. Munk and C. Wunsch. Ocean acoustic tomography: a scheme for large scale monitoring. *Deep Sea Research Part A. Oceanographic Research Papers*, 26(2):123–161, 1979.

[16] W. Munk and C. Wunsch. Ocean acoustic tomography: a scheme for large scale monitoring. *Deep Sea Research Part A. Oceanographic Research Papers*, 26(2):123–161, 1979.

[17] W. Munk and C. Wunsch. Ocean acoustic tomography: a scheme for large scale monitoring. *Deep Sea Research Part A. Oceanographic Research Papers*, 26(2):123–161, 1979.

[18] W. Munk and C. Wunsch. Ocean acoustic tomography: Rays and modes. *Reviews of Geophysics*, 21(4):777–793, 1983.

[19] Nobska Development Corporation. *MAVS3 Operations Manual*, 4.5 edition.

[20] G. of Canada. Fisheries and oceans canada: Tides, currents and water levels, 2019.

[21] M. Razaz, K. Kawanisi, I. Nistor, and S. Sharifi. An acoustic travel time method for continuous velocity monitoring in shallow tidal streams. *Water Resources Research*, 49, 08 2013.

[22] S. C. Riser, H. J. Freeland, D. Roemmich, S. Wijffels, A. Troisi, M. Belbéoch, D. Gilbert, J. Xu, S. Pouliquen, and A. e. a. Thresher. Fifteen years of ocean observations with the global argo array. *Nature Climate Change*, 6(2):145–153, 2016.

[23] D. Shepard. A two-dimensional interpolation function for irregularly-spaced data. In *Proceedings of the 1968 23rd ACM National Conference*, ACM '68, pages 517–524, New York, NY, USA, 1968. ACM.

[24] J. L. Spiesberger. Us patent 5691957: Ocean acoustic tomography, 1997.

[25] F. T. Thwaites and A. J. Williams. Development of a modular acoustic velocity sensor. In *OCEANS 96 MTS/IEEE Conference Proceedings. The Coastal Ocean - Prospects for the 21st Century*, volume 2, pages 607–612 vol.2, Sep. 1996.

[26] J. Truchsess. Simple circuit communicates over low-voltage power lines, 2019.

[27] A. Williams. Development of an acoustic current meter: Lessons taught by clients and colleagues. http://www.nobska.net/resources/PAPERS/2010-Oceans-Seattle-Lessons-Taught.pdf.

[28] A. J. Williams, F. T. Thwaites, A. T. Morrison, J. M. Toole, and R. Krishfield. Motion tracking in an acoustic point-measurement current meter. In *OCEANS'10 IEEE SYDNEY*, pages 1–8, May 2010.